Entry of cell-penetrating peptide transportan 10 into a sinlge vesicle of lipid membranes and its induced pore formation

DOCTORAL THESIS

Entry of cell-penetrating peptide transportan 10 into a single vesicle of lipid membranes and its induced pore formation

Supervisor: Prof. Masahito Yamazaki

Md. Zahidul Islam

Student ID No.: 55244015

Department of Bioscience,

Graduate School of Science and Technology,

Shizuoka University, Shizuoka, Japan.

August, 2015.

Abstract

Plasma membranes of eukaryotic cells prevent the entry of biomacromolecules inside the cells. Cell-penetrating peptides (CPPs) have an ability to translocate across the plasma membranes to enter into cells. Transportan 10 (TP10), a synthetic CPP, has a cell-penetrating activity and thus can be used for the intracellular delivery of biological cargo such as proteins and oligonucleotides. However, the mechanisms of translocation and the delivery of large cargo molecules are still controversial. Many researchers investigated the interactions of TP10 with lipid membranes using a suspension of large unilamellar vesicles (LUVs). However due to the disadvantage of the LUV suspension method, elementary processes of the interaction of TP10 with lipid membranes remain unclear. In this thesis, the entry of TP10 into a single giant unilamellar vesicle (GUV) and the TP10-induced pore formation were investigated using the single GUV method.

[Chap.2]: To investigate the entry of TP10 into a GUV and the TP10-induced pore formation, a new method was developed to detect the entry of TP10 into a GUV using confocal microscopy. Using this method, interactions of carboxyfluorescein (CF)-labeled TP10 (CF-TP10) with single GUVs containing a water-soluble fluorescent dye, Alexa Fluor 647 hydrazide (AF647) and smaller vesicles were investigated. As lipid membranes, 20% dioleoylphosphatidylglycerol (DOPG) /80% dioleoylphosphatidylcholine (DOPC) was used. After starting the interaction of CF-TP10 with a GUV, the fluorescence intensity of the GUV membrane increased with time to a saturated value, then the fluorescence intensity due to the membranes of the smaller vesicles inside the GUV increased prior to leakage of AF647. This result indicates that CF-TP10 entered the GUV from the outside by translocating across the lipid membrane before CF-TP10-induced pore formation. The fraction of entry of CF-TP10 inside the GUVs before pore formation increased with an increase in CF-TP10 concentration and became

1.0 at and above 1.0 μM. The rate constants of CF-TP10-induced pore formation in lipid membranes were determined, which were larger than these TP10. Large molecules such as Texas Red dextran 40000, and vesicles with a diameter of 1-2 μm, permeated through the TP10-induced pores or local rupture in the lipid membrane. The interaction of CF-TP10 with single DOPC-GUVs were also investigated and essentially identical results as for 20%DOPG/80%DOPC-GUVs were obtained. These results provide the first direct experimental evidence that TP10 can deliver large cargo through lipid membrane.

[Chap.3] Plasma membrane of eukaryotic cells contain high concentrations of cholesterol. It is well known that there are many effects of cholesterol (chol) on physical properties of membrane. Thereby it is important to elucidate the effect of cholesterol on entry of TP10. The effect of cholesterol on the entry of TP10 into single GUVs of DOPG/DOPC/chol mixture and the TP10-induced pore formation in the membranes were investigated. CF-TP10 entered single GUVs of the membranes containing high concentrations of cholesterol before leakage of AF647, although a little higher concentrations of CF-TP10 were required for the entry compared with membranes without cholesterol. This result indicates that TP10 can translocate across lipid membrane regions in plasma membranes of eukaryote.

[Chap.4] The effects of stretching of lipid membranes on the entry of TP10 into single 20%DOPG/80%DOPC-GUVs and the TP10-induced pore formation were investigated. The binding of TP10 to a GUV membrane induced stretching of the membrane and during an increase in stretching pore formation occurred stochastically in the membrane. The fractional area change of a GUV membrane played an important role in the TP10-induced pore formation. Tension due to the external force decreased TP10-concentration required for the pore formation, and also increased the fraction of entry of CF-TP10 into a GUV before pore formation, and hence the rate of entry of CF-TP10 into a single GUV was increased.

The elementary processes of the entry of TP10 into a single vesicle and the TP10-induced pore formation in the lipid membrane were revealed. Based on the experimental results, it is concluded that the TP10 can enter GUVs of lipid membrane before TP10-induced pore formation. Therefore, TP10 can be used as a vector to deliver large cargo through lipid membranes without the need for special transport mechanisms such as those found in cells.

Contents

List of Tables

List of Figures

List of Abbreviations

Abbreviation	Meaning
CPP	Cell-Penetrating Peptide
GUV	Giant Unilamellar Vesicle
LUV	Large Unilamellar Vesicle
SUV	Small Unilamellar Vesicle
TP	Transportan
TP10	Transportan 10
CF	Carboxyfluorescein
DOPC	Dioleoylphosphatidylcholine
DOPG	Dioleoylphosphatidylglycerol
Chol	Cholesterol
TRD	Texas Red Dextran
AF647	Alexa Fluor 647 hydrazide
BSA	Bovine serum albumin
CLSM	Confocal Laser Scanning Microscopy
HIV	Human Immunodeficiency Virus
Biotin Lipid	N-((6-(biotinoyl)amino)-hexanoyl)-1,2-dihexadecanoyl-*sn*-glycero-3-phosphoethanolamine, triethyl ammonium salt (biotin-X-DHPE)
F-NMR	Fluorine-19 nuclear magnetic resonance
POPC	Palmitoyl-oleoyl-phosphatidylcholine
DMPC	Dimyristoly phosphatidylcholine
Tat	Trans-Activator of Transcription
LTR	Long Terminal Repeat

Chapter-1

General Introduction

1.1 WHAT ARE CELL PENETRATING PEPTIDES (CPPs)?

Plasma membranes or biomembrane prevent the entry of pharmacologically active biomacromolecules. Biomembranes are generally impermeable to polypeptides and oligonucleotides (Foerg and Merkle, 2008). A new kind of peptides that can translocate across the plasma membranes and enter cells has been found for last a few decades. These peptides are very short (not more than 30 to 35 amino acid residues), polybasic, mostly positively charged, and they have a high solubility in water. These peptides are called cell-permeating or cell-penetrating peptides (CPPs) (Foerg and Merkle, 2008). Most of the CPPs can bind with plasma membranes and internalize into a cell without a receptor or a transport system (Figure-1.1). The mechanism of translocation of CPPs across the plasma membranes is still controversial. Some CPPs internalize via endocytosis, but others use non-endocytotic pathways for their translocation to enter into cells (Figure-1.2). CPPs are capable of delivering cargo molecules into cells and these cargo molecules sometimes are larger than the CPPs themselves (Dietz & Bähr, 2004). Thereby, CPPs can be used as a vector to deliver the drugs, chemicals, or proteins into cells for curing the infections (Delcroix and Riley, 2010).

At the early stage of the research of CPPs, the translocation of CPPs into cells had been examined using fixed cells. Most of the experimental results showed that the CPPs can translocated the plasma membranes to enter into cells and finally reached at the nucleus of cells. For example, the penetratin, one of the CPPs, translocated through the cell membranes and internalized into the nucleus at room temperature and 4 °C by non-endocytotic pathways (Derossi et al., 1994). The cell fixation is a process to stop the life activity of a cell.

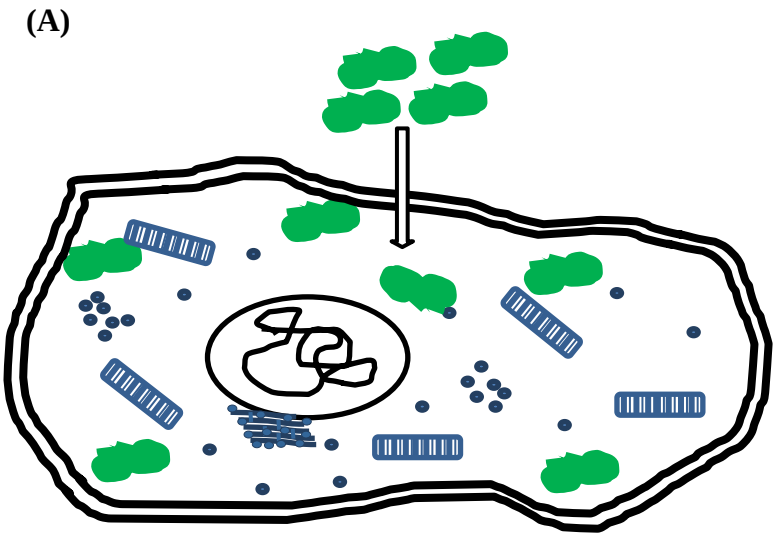

Figure-1.1: CPPs translocate the plasma membrane and internalize into a cell.

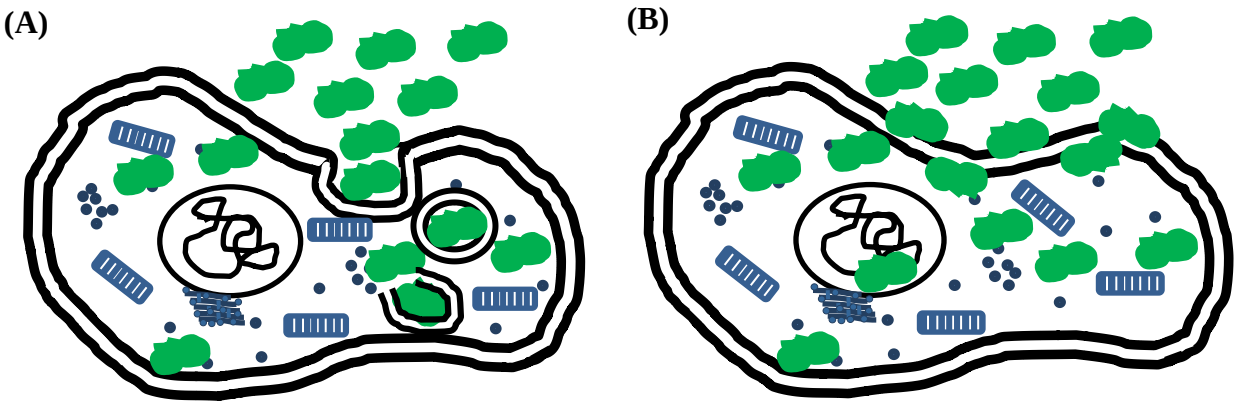

Figure-1.2: CPPs translocate across the cell membrane by (A) endocytosis process and (B) non-endocytosis process.

For cell fixation, first culture media is removed from cells and the cells are washed with specific buffer solution. Then the fluorescence probe-labeled peptide solution is incubated with cells for a few minutes. Extra peptides are washed away with buffer and then formaldehyde or glutaraldehyde is added into the solution of the cells to fix the cell structure. Then cells are washed with buffer solution and finally the fixed cells are observed using fluorescence microscopy. It turned out that the cell fixation affects the membrane permeation and peptides move to the new location because the result of CPPs translocation in living cells was different from fixed cell method (Fuchs & Raines, 2004; Maiolo et al., 2005). Thereby, the cell fixation method greatly affects the accurate measurement of translocation of CPPs into cells. Then many scientists started to re-examine the translocation of various CPPs using living cells. For example, the results using living cells show that the fluorescence probe-labeled penetratin translocated across the membrane of living K562 cells by endocytotic pathways, which indicates that the previous conclusion obtained using the fixed cell method was wrong (Drin et al., 2003; Fischer et al., 2004).

CPPs are classified to non-amphipathic, primary amphipathic, secondary amphipathic, and hydrophobic groups based on the peptide sequence and physico-chemical properties (Milletti, 2012). Non-amphipathic peptides such as octa-arginine (R8) nona-arginine (R9) are very short peptides, which consist of several positively-charged arginine residues. It is considered that polyarginine mainly binds the phosphate group of phospholipids (Mishra et al., 2011). Primary amphipathic peptides consist of a hydrophilic segment and a hydrophobic segment and the latter segment binds with cell membranes. Secondary amphipathic peptides shows their amphipathicity after forming a helical or a beta sheet structure in lipid membrane (Madani et al., 2011). Hydrophobic peptides can translocate through cell membranes but their amino acid sequence does not affect their translocation. Some hydrophobic peptides form a staple structure in the membrane interface and its help their translocation (Milletti, 2012). On the other hands, CPPs are

also classified according to their origin, such as protein-derived peptides, and chimeric peptides (Magzoub & Gräslund, 2004). The detailed classification of CPPs are given in Table-1.1 and 1.2.

Historically, Tat (Trans-Activator of Transcription) is the first peptide recogniged as a CPP. Green and Loewenstein found that Tat protein (86 amino acids) encoded from the human immunodeficiency virus (HIV) type-1 has an ability to be internalized into cells. Tat translocated across the cell membrane and entered into the nucleus, which activated HIV long terminal repeat (HIV-LTR) (Green and Loewenstein, 1988). Frankel and Pobo also found that the Tat protein translocated through the cell membrane and internalized in the cytosol and finally entered into the nucleus of the cells (Frankel and Pobo, 1988). In the interaction of various fluorescence probe-labeled truncated HIV-1 Tat peptides with living HeLa GH cells, Tat peptides were localized into cells nucleus within a few minutes after mixing with cells (Vivès et al., 1997).

Poly arginine peptides such as R9 have an activity of cell penetration; R9 translocated across the living cell membrane using endocytotic pathway (Fuchs & Raines, 2004). Fischer et al. used the living MC57 cells for the examination of entry of Fluo-penetratin, Fluo-Tat, and Fluo-R9 into cells. All the peptides were localized in the cytosol of the living cells (Fischer et al., 2004). The translocation efficiency decreased by the attachment of cargo molecule with hepta-arginine, R7 (Maiolo et al., 2005).

There are various kinds of synthetic chimeric CPPs such as transportan (TP), which are designed by the fusion of two peptides sequence collected from different sources (Soomets et al., 2000 and Langel et al., 1996). TP is a well-known fusion or chimeric CPP; N-terminal 13 amino acids of TP come from galanin and C-terminal 14 amino acids from mastoparan. Galanin is a neuropeptide widely found in the brain and spinal cord of humans and other mammals. Mastoparan is a toxin from wasp venom and it simulates the exocytosis of different kinds of mammalian cells. Transportan 10 (TP10) (21 amino acids) is a truncated analogue of TP (27 amino acids) by the deletion of six amino acids from the N-terminus of TP. TP and TP10

Table-1.1: Physico-chemical properties-based classification of CPPs:

Types of peptide	Example of the peptide	Sequence of peptide	Reference
Non-amphipathic	R8	RRRRRRRR	Okamura et al., 2005
	R9	RRRRRRRRR	Fischer et al., 2004
Primary amphipathic	MPG	GLAFLGFLGAAGSTMGAWSQPKKKRKV	Simeoni et al., 2003
	Pep-1	KETWWETWWTEWSQPKKRKV	Morris et al., 2001
Secondary amphipathic	MAP	KLALKALKALKAALKLA	Oehlke et al., 2004
	GALA	WEAALAEALAEALAEHLAEALAEALEALAA	Li et al., 2004
Hydrophobic	Pept1	PLILLRLLRGQF	Marks et al., 2011
	Pept2	PLIYLRLLRGQF	Marks et al., 2011

Table-1.2: Origin-based classification of CPPs:

Types of peptide	Example of the peptide	Sequence of peptide	Reference
Protein derived	Tat(48-60)	GRKKRRQRRRPPQ	Vivès et al., 1997
	Penetratin	RQIKIWFQNRRMKWKK	Drin et al., 2003
Antimicrobial	Buforin II	TRSSRAGLQWPVGRVHRLLRK	Kobayashi et al., 2000
	$Bac7_{15-24}$	PRPLPFPRPG	Sadler et al., 2002
Chimeric	Transportan	GWTLNSAGYLLGKINLKALAALAKKIL	Padari et al., 2005
	TP10	AGYLLGKINLKALAALAKKIL	Padari et al., 2005
Prion	MPrPp(1-28)	MANLGYWLLALFVTMWTDVGLCKKRPKP	Oglęcka et al., 2008

translocated across the cell membrane of epithelial Caco-2 cells more effectively than penetratin (Lindgren et al., 2004).

There are some antimicrobial peptides which have a cell penetrating activity. These peptides can be used as a vector molecule to transfer various types of cargo molecules (proteins and oligonucleotides) into cells. The most intensive studies have been done on the synthetic CPP model amphipathic peptide (MAP). MAP formed secondary structure when bound with plasma membrane and showed the amphipathic character. This secondary structure is necessary for their translocation and internalization into cells (Scheller et al., 1999).

1.2 INVESTIGATION OF INTERACTION OF CPPS WITH LIPID MEMBRANES:

To elucidate the mechanism of translocation and entry of CPPs into cells, interaction of CPPs with lipid membranes have been investigated using a suspension of small liposomes such as large unilamellar vesicles (LUVs) or small unilamellar vesicles (SUVs) whose diameters are less than 200-300 nm (the LUVs suspension method). In this method, various physico-chemical parameters such as fluorescence intensity of the LUVs interacting with CPPs are measured. The fluorescence probe-labeled penetratin and related peptides applied in the neutral and negatively-charged lipid LUVs suspension. For example, penetratin and related peptides bound with LUVs of neutral lipids and negatively-charged lipid mixture, and translocated across the LUV membranes only in presence of transmembrane potential (Terrone et al., 2003). Jobina et al. examined the interaction of CPP RW16 (derived from penetratin) with LUVs of electrically neutral and negatively-charged lipid mixture. They found that the RW16 peptide associated with each other and formed oligomer, and this oligomerization is essential for the interaction with lipid membranes. They also observed that this peptide strongly interacts with negatively-charged lipid membranes compared with neutral ones (Jobina et al., 2013). On the other hand, the experimental results of interaction of buforin 2 with LUVs show that this peptide is not effectively released the entrapped fluorescent dyes from inside of the LUVs. However, buforin 2

has an activity to translocate across lipid bilayers (Kobayashi et al., 2000).

1.3 INTERACTION OF TP OR TP10 WITH CELLS OR LUVS:

Interaction of TP or TP10 with cells or unilamellar vesicles has been investigated by many scientists. The TP and its analog (TP10) with cargo molecules (fluorescent-labeled avidin or streptavidin-gold conjugates) translocated across the plasma membranes and entered into cell. Within very short time TP or TP10 with cargo molecules were present in endocytic vesicles and later it localized in the perinuclear region (Padari et al., 2005). TP10 attached with Myc protein as a cargo molecules easily translocated across the plasma membranes and accumulated in the cytosol by non-endocytotic process. Since TP10 translocated across the plasma membranes in presence of endocytosis inhibitor, it is considered that the translocation of TP10 to cells occurs through non-endocytotic pathway (EL-Andaloussi et al., 2005).

The binding of TP10 with lipid membranes and TP10-induced leakage of fluorescent probes from LUVs have been investigated using the LUV suspension method. Interaction of TP10 with LUVs induced gradual leakage of the fluorescent probes from the lumen of phospholipid vesicles (Yandek et al., 2007). The attachment of cargo molecules with TP10 decreased the leakage of the internal content (Fluorescence probe) of palmitoyl-oleoyl-phosphatidylcholine (POPC)-LUVs (Bárány-Wallje et al., 2007). The thermodynamics and kinetics of binding of TP10 and different mutant TP10 with lipid membranes also examined. The binding activity of a TP10 analogue (replacement of Tyr with Trp) with phospholipid membrane was larger than TP10. They also found that the binding and dye efflux rate also increased with an increase in the fraction of negatively-charged lipid in the membranes (Yandek et al. 2008).

Molecular dynamics simulation study indicates that TP10 forms a random coil structure in water but its form an α-helical structure upon binding with a POPC bilayer (Dunkin et al., 2011). Recent study using F-NMR (Fluorine-19 nuclear magnetic resonance) and circular

dichroism analysis indicates that the N-terminus of TP10 was flexible but its C-terminus formed an α-helical structure when TP10 bound with the lipid membrane (Fanghänel et al., 2014).

The interaction of fluorescence probe-labeled TP10 and its analogue with HeLa cells and NIH-3T3 cells were examined using flow cytometry. The results show that the translocation ability of TP10 analogues into cells increased with an increase in the number of positively-charged amino acids in the TP10 analogues (Song et al., 2011). The TP10 containing cargo molecules [LXXLL-motif of the human SRC-1nuclear receptor box 1 (TP10-SRC1$_{LXXLL}$)] has an ability to enter into MCF-7 cells. The TP10-SRC1$_{LXXLL}$ decreased the growth of breast cancer cell after it enter into the affected cells (Tints et al., 2014).

1.4 PURPOSE OF THE RESEARCH:

To elucidate the mechanism of the entry of CPPs into cells, it is important to investigate the interactions of CPPs with lipid membranes. As described in previous section, the interactions of CPPs such as TP10 with lipid membranes have been investigated using the LUV suspension method. However, when the LUV suspension method is used, the average values of the physical parameters of liposomes are obtained from a large number of liposomes and thereby much information has been lost. Especially, it is difficult to obtain the information of elementary processes of reactions and structural changes occurred in lipid membranes. Recently, giant unilamellar vesicles (GUVs) of lipid membranes with diameter greater than 10 μm have been used for the investigation of physical properties of lipid membranes such as elasticity, shape change and phase separation. The advantages of GUVs is that the structural and physical properties of GUVs can be observed in real time. Recently, Yamazaki et al. have developed the single GUV method to investigate the functions and dynamics of biomembranes. In this method, changes in the structure and physical properties of a single GUV that are induced by interactions of compounds such as peptides/proteins with the lipid membrane are observed as a function of time and spatial

coordinates. The same experiment is repeated many times using other single GUVs. The results are used to analyze statistically the changes in the physical properties of a single GUV to obtain rate constants for the elementary processes underlying the structural changes and functions of GUVs. This single GUV method can reveal details of the elementary processes of individual events, and allow calculation of their kinetic constants (Yamazaki, 2008). Using the single GUV method, the rate constants of pore formation in lipid membranes induced by the antimicrobial peptide magainin 2 and the rate constant of membrane permeation of various fluorescent probes through these pores have been obtained (Tamba & Yamazaki, 2005; Tamba & Yamazaki, 2009; Tamba et al., 2010, Karal et al., 2015a). This method allows to distinguish pore formation step in membranes from the step of fluorescent probe leakage through the pores, which enables an accurate estimation of the rate constants of both the elementary processes (Tamba et al., 2010).

In this thesis, to understand the mechanism of translocation of TP10 across the plasma membrane into cells, the interactions of TP10 with lipid membranes were investigated using the single GUV method.

In chapter 2, a new method was developed to investigate the translocation of TP10 across a lipid membrane into single GUVs. Using this method the relationship between the entry of TP10 and the TP10-induced pore formation was investigated. To estimate quantitatively these phenomena, the fraction of entry of TP10 into a GUV at a specific time and the rate constant of pore formation were used. The size of the TP10-induced pore was also investigated.

In chapter 3, the effects of cholesterol on the entry of TP10 into a GUV and its pore formation were investigated using the method developed in chapter 2.

In chapter 4, to elucidate the mechanism of the entry of TP10 into a single GUV and its pore formation, the TP10-induced area change of a GUV membrane and the effect of stretching on the entry of TP10 into a GUV were investigated.

Chapter-2

Entry of cell-penetrating peptide transportan 10 into a single vesicle by translocating across lipid membrane and its induced pores.

2.1 INTRODUCTION:

As described in chapter 1, TP10 is one of the CPPs. TP10 can deliver a large protein such as an antibody, oligonucleotide, and colloidal gold (diameter 10 nm) as cargo (E.L.–Andaloussi et al., 2005). The TP10 and its different analog containing positively charged amino acid can enter into the live cell (Song et al., 2011). The TP10 containing cargo molecules can translocate across the cell membrane and enter into the cytoplasm and nucleus of the living cell. (Tints et al., 2014).

The interaction of TP10 with lipid membranes has been investigated using a suspension of small liposomes (LUVs) (the LUV suspension method) (Yandek et al., 2007; Yandek et al., 2008; Barany-Wallje et al., 2007). TP10 induced gradual leakage (diffusion) of a small water-soluble fluorescent probe, carboxyfluorescein, from the inside to the outside of LUVs in a concentration-dependent manner (Yandek et al., 2007). TP10 bound to the outer monolayer of the lipid vesicles and perturbed due to the TP10 concentration difference between the outer and inner monolayer. TP10 translocated across the lipid bilayer during perturbation. Results from fluorescence ANTS/DPX assays suggested that the leakage of fluorescent probes is “graded”. The data were analyzed assuming that the leakage of these fluorescent probes occurs during the translocation of TP10 across the lipid bilayer (Yandek et al., 2007; Yandek et al., 2008). This state was defined as the TP10-induced pore in the lipid membrane. The replacement of Tyrosine amino acid with Tryptophan from the TP10 peptide enhanced the binding activity and dye release (Yandek et al., 2008). TP10 formed the α-helices structure when embedded in the

membrane (Fanghänel et al., 2014). However, in the LUV suspension method, the average values of the physical parameters of the liposomes are obtained from a large number of liposomes which are in different elementary steps of the peptide-induced structural change, and therefore much information is lost (Yamazaki, 2008; Tamba et al., 2007). Moreover, the LUV suspension method does not allow determination of the main cause of leakage because many factors could be involved, such as pore formation, membrane fusion, rupture, and fragmentation of liposomes. These structural changes cannot be directly detected in LUVs in suspension. It is therefore difficult to identify the mechanism of translocation of TP10 across the lipid membrane, and the mechanism of TP10-induced leakage of fluorescent probes, using only the LUV suspension method.

Recently, giant liposomes or giant unilamellar vesicles (GUVs) with diameters greater than 10 μm have been used to investigate the physical properties of vesicle membranes, such as shape change and phase separation (Saitoh et al., 1998; Baumgart et al., 2003). The shape of a single GUV and its physical properties in water can be measured in real time. Based on the characteristics of these GUVs, we have developed a single GUV method to investigate the functions and dynamics of biomembranes (Yamazaki, 2008; Tamba & Yamazaki, 2005; Tamba & Yamazaki, 2009; Tamba et al., 2010; Alam et al., 2012; Tamba et al., 2007; Tanaka et al., 2004) . Using this method, changes in the structure and physical properties of a single GUV induced by interactions with materials such as peptides and proteins are observed as a function of time and spatial coordinates. Then, the same experiments are repeated many times using other single GUV. The results are used to analyze statistically the changes in the physical properties of a single GUV to obtain rate constants of elementary processes for reactions of GUVs. For example, we studied peptide/protein-induced leakage (i.e., membrane permeation) of the internal contents (such as water-soluble fluorescent probes) from single GUVs using the single GUV method. This enabled identification of the cause of leakage and calculation of the rate constants of elementary

processes involved in leakage (such as peptide/protein-induced pore formation in lipid membranes, and leakage of fluorescent probes through the pores) (Yamazaki, 2008). We have determined the rate-constants of pore formation in lipid membranes induced by the antimicrobial peptide magainin 2 and the pore-forming toxin lysenin, and also the rate constant of membrane permeation of various fluorescent probes through these pores. These results have provided valuable information revealing the mechanisms of pore formation (Tamba & Yamazaki, 2005; Tamba & Yamazaki, 2009; Tamba et al., 2010; Alam et al., 2012).

In the present study, we used the single GUV method to investigate the translocation of TP10 across a lipid membrane into a GUV, and TP10-induced leakage of a water-soluble fluorescent probe from the inside to the outside of a GUV. Specifically, we investigated the translocation of a fluorescent probe, carboxyfluorescein (CF)-labeled TP10 (CF-TP10), across the lipid membrane and the leakage of a water-soluble fluorescein probe, Alexa Fluor 647 hydrazide (AF647), from 20% dioleoylphosphatidylglycerol (DOPG)/80% dioleoylphosphatidylcholine (DOPC)-GUVs simultaneously using confocal laser scanning microscopy (CLSM). To elucidate the translocation of TP10 with cargo molecules, we also investigated the permeation of larger molecules such as the fluorescent probe, Texas Red (TR)-labeled dextran 40K (TRD-40k) (Tamba et al., 2010) and lipid vesicles through the membranes. In addition, TP 10-induced structural changes of GUVs were studied. Based on the results, we discuss the fundamental steps by which TP10 translocates the lipid membrane and induces pore formation.

2.2 MATERIALS AND METHODS:

DOPC and DOPG were purchased from Avanti Polar Lipids Inc. (Alabaster, AL) (Figure-2.1). Bovine serum albumin (BSA) was purchased from Wako Pure Chemical Industry Ltd. (Osaka, Japan). AF647, TRD-10k, TRD-40k, and N-((6-(biotinoyl)amino)-hexanoyl)-1,2-dihexadecanoyl-*sn*-glycero-3- phosphoethanolamine, triethyl ammonium salt (biotin-X-DHPE,

referred to as biotin-lipid) were purchased from Invitrogen Inc. (Carlsbad, CA). Calcein was purchased from Dojindo Laboratory (Kumamoto, Japan). Biotin-labeled BSA and streptavidin were purchased from Sigma-Aldrich Co. (St. Louis, MO, USA). TP10 was synthesized by the FastMoc method using a 433A peptide synthesizer (PE Applied Biosystems, Foster City, CA). The sequence of TP10 (21-mer) is AGYLLGKINLKALAALAKKIL and has an amide-blocked C terminus. The fluorescence probe carboxyfluorescein-labeled TP10 (CF-TP10), which has one fluorophore CF at the N-terminus of the peptide, was synthesized using a standard method (Thorén et al., 2000) by the reaction of 5-(and 6)-carboxyfluorescein succinimidylester (Invitrogen) (19 mg) with TP10-peptide resin (80 mg) (molar ratio of reagent to peptide: 2.5 to1) in dimethylformamide for 24 h at room temperature. TP10 and CF-TP10 were cleaved from the resin using trifluoroacetic acid, 1,2-ethanedithiol, and MilliQ water (9.5/0.25/0.25, volume ratio). The methods for purification and identification of these peptides were described previously (Tamba & Yamazaki, 2005; Tamba & Yamazaki, 2009; Tamba et al., 2010). The purified peptides were analyzed by ion-spray ionization mass spectrometry using a single quadrupole mass spectrometer (API 150*EX*, *PE SCIEX*, PE Applied Biosystems). The measured mass of TP10 and CF-TP10 was 2181 ± 1 Da and 2540 ± 1 Da, respectively, which correspond to the molecular mass calculated from the amino acid composition.

(A)

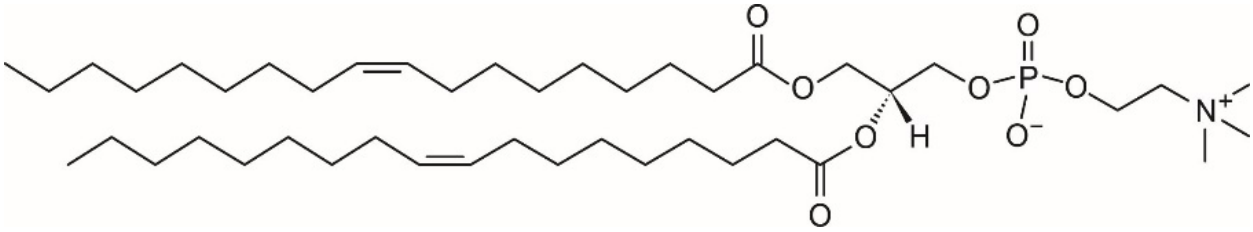

(B)

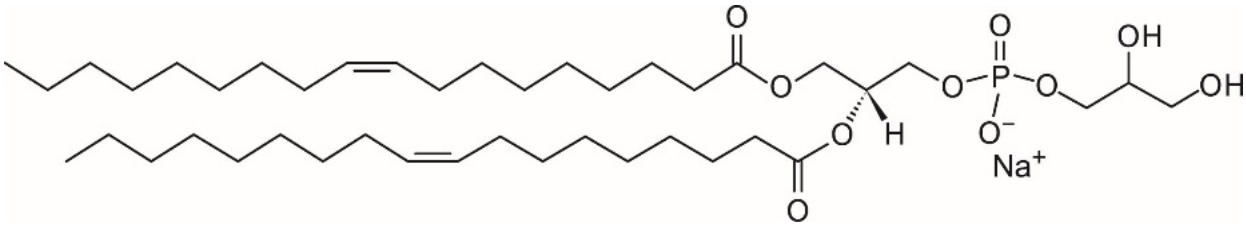

Figure-2.1: Structure of DOPC (A) and DOPG (B) lipid molecule ("Structures shown above kindly supplied by Aventi Polar Lipids, Inc.").

GUVs of DOPG/DOPC/biotin-lipid (molar ratio: 20/79/1, referred to as 20%DOPG/79%DOPC/1%biotin-lipid) were prepared by incubation of buffer H (10 mM HEPES, pH 7.5, 150 mM NaCl, and 1 mM EGTA) containing 0.1 M sucrose and various fluorescent probes with dry lipid films by the natural swelling at 37 °C (Tamba & Yamazaki, 2005; Tamba & Yamazaki, 2009; Tamba et al., 2010;). The concentrations of the fluorescent probes were: 6 μM for AF647, 10 μM for TRD-10k, 10 μM for TRD-40k, and 1 mM calcein. To prepare GUVs containing smaller vesicles, a GUV suspension was prepared in a buffer containing no fluorescent probes using the above method, then the GUV suspension was centrifuged at 14,000 × g for 20 min at 20 °C to remove multilamellar vesicles and lipid aggregates. A mixture of the partially purified GUV suspension and AF647 solution in buffer H containing 0.1 M sucrose was incubated with dry lipid films at 37 °C. The membrane filtering method was used to remove untrapped fluorescent probes (Tamba et al., 2011).

Purified GUV suspension (300 μL: 0.1M sucrose in buffer H as the internal solution; 0.1M glucose in buffer H as the external solution) was transferred into a hand-made microchamber (Yamazaki, 2008; Tamba, Y., and Yamazaki, 2005). Single GUVs were fixed on a slide glass or a coverslip in the chamber using the strong association between biotin and streptavidin, previously used to fix LUVs onto glass surfaces (Stamou et al., 2003). First, 0.9 mg/mL BSA and 0.1 mg/mL biotin BSA in buffer H containing 0.1 M glucose were added to the chamber and incubated. Excess biotin BSA and BSA were removed by washing with the same buffer, leaving a BSA/biotin-BSA coating on the glass surface of the chamber. Next, 0.025 mg/mL streptavidin and 0.1 mg/mL BSA in the same buffer were added to the chamber and incubated, then removed using the same buffer. Finally, a suspension of GUVs containing biotin-lipid was transferred into the chamber. Due to the strong binding of streptavidin with both the biotin-BSA adsorbed on the glass surface and the biotin-lipid in the GUV membrane, the GUV was connected to the glass surface via a tether comprising a long hydrophilic segment of

biotin- lipid.

The concentration of TP10 solution in buffer H determined by the absorbance at 280nm for single tyrosine amino acid in UV spectrophotometer (VU-1800, Shimadzu, Japan). By using Beer's Law [Abs = ε c L or Abs = ε c when L = 1 cm; where, ε: molar extinction coefficient (1280 for Tyr), c: Concentration, L: light path length in centimeters] we can calculate the TP10 concentration. We also used the same equation for the calculation of CF-TP10 concentration. We took the absorbance of CF-TP10 at 492 nm for carboxyfluorescein and used ε = 81000 for the calculation of concentration of CF-TP10.

The GUVs were observed using a CLSM (FV-1000, Olympus, Tokyo, Japan) or an inverted fluorescence phase contrast microscope (IX-70, Olympus) at 25 ± 1 °C using a stage thermocontrol system (Thermoplate, Tokai Hit, Shizuoka, Japan). For CLSM measurements, fluorescence images of AF647 (excited by a laser at λ = 633 nm) and of CF-TP10 (excited by a laser at λ = 488 nm) were obtained using a 60× objective (UPLSAPO060X0, Olympus) (NA = 1.35). For measurements using IX-70, phase contrast and fluorescence images of GUVs were recorded using a high-sensitivity fluorescence camera (EM-CCD camera, C9100-12, Hamamatsu Photonics K.K., Hamamatsu, Japan) containing a hard disk. Three ND filters were used to decrease the intensity of the incident light to reduce photobleaching of fluorescent probes. The fluorescence intensity inside the GUVs was determined using an Aqua Cosmos (Hamamatsu Photonics K.K.) and the average intensity per GUV was estimated. During the interaction of peptides with a single GUV, various concentrations of CF-TP10 or TP10 in buffer H containing 0.1 M glucose were added continuously to the vicinity of the GUV through a 20-μm-diameter glass micropipette positioned by a micromanipulator. The distance between the GUV and the tip of the micropipette was 50-60 μm. The details of this method were described previously (Yamazaki, 2008; Tamba & Yamazaki, 2005; Tamba & Yamazaki, 2009; Tamba et al., 2010; Alam et al., 2012; Tamba et al., 2007; Tanaka et al., 2004).

Obtaining the time course of the fluorescence intensity required special methodology because the GUVs were not fixed at one position, but rather moved slightly (less than 10 μm) during interaction with CF-TP10 (or TP10). To measure the time course of the fluorescence intensity of AF647 inside a GUV, we specified a larger region encompassing the entire area occupied by the GUV during the interaction of CF-TP10 (or TP10) and measured the fluorescence intensity of this area as a function of time. To measure the time course of the CF-TP10 fluorescence intensity at the rim of the GUV (i.e., the GUV membrane), a vertical line was drawn through the center of each GUV (Figure 2.2(A)) and the fluorescence intensity profile along the line was measured (Figure 2.2(B)). The two points with the highest intensity correspond to the GUV membrane; therefore, the average value of the intensity of the two points was taken as the fluorescence intensity of the GUV membrane. Typically, the fluorescence intensity of the rim of the GUV was measured every 10 s. For these analyses we used only GUVs with a diameter of 30-40 μm. To obtain the rate constant of CF-TP10 (or TP10)-induced pore formation (k_P), 3 independent experiments were carried out for each CF-TP10 or TP10 concentration using 20-30 single GUVs. Average values and standard errors of k_P were calculated.

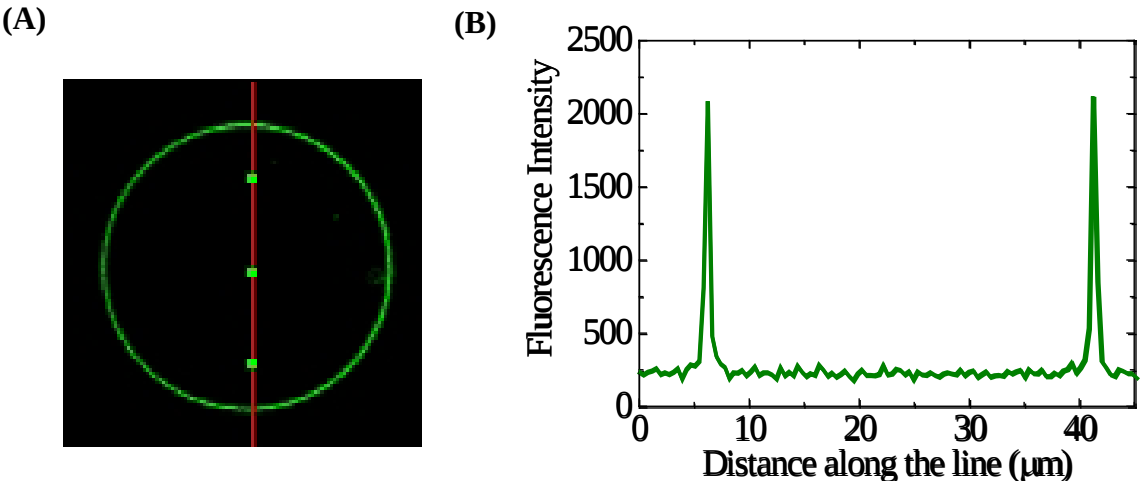

Figure-2.2: Measurement of the fluorescence intensity of the rim of a GUV (the GUV membrane) due to CF-TP10. A vertical line which goes through the centre of the GUV was drawn for each GUV (Figure (A)). The green circle corresponds to the GUV membrane and the red line corresponds to the vertical line. Figure (B) shows a fluorescence intensity profile along the line. The two points with the highest intensity correspond to the GUV membrane. The average value of the intensity of these two points was taken as the fluorescence intensity of the GUV membrane.

2.3 RESELTS AND DISCUSSION:

2.3.1 Translocation of CF-TP10 across the lipid membrane of GUVs before pore formation:

We first investigated the interaction of CF-TP10 with single 20%DOPG/79%DOPC/ 1%biotin-lipid-GUVs containing AF647 using CLSM. The interaction was carried out in buffer H containing 0.1 M glucose at 25 °C and was analyzed using the single GUV method. Figure 2.3A shows a typical result of the effect of the interaction of 1.9 μM CF-TP10 with single GUVs. The CF-TP10 solution was continuously provided to the GUV surroundings through a micropipette, so the equilibrium CF-TP10 concentration near the GUV was essentially the same as that in the micropipette (Tamba & Yamazaki, 2009; Tanaka et al., 2004). A fluorescence microscope image of the GUV (Figure 2.3A (1)) shows a high concentration of AF647 inside the GUV. During the addition of the 1.9 μM solution of CF-TP10, the fluorescence intensity inside the GUV remained essentially constant over the first 212 s, after which the fluorescence intensity gradually decreased (Figure 2.3A (1) & red curve in Figure 2.3B). After 310 s, the fluorescence intensity was 30% of the initial intensity (at $t = 0$), although a fluorescence microscope image of the same GUV due to CF-TP10 (Figure 2A(2)) shows that the GUV was intact and spherical. As discussed in our reports on magainin 2 and lysenin (Tamba & Yamazaki, 2005; Tamba & Yamazaki, 2009; Tamba et al., 2010; Alam et al., 2012), the decrease in fluorescence intensity results from the leakage of AF647 from the GUV through CF-TP10-induced pores in the membrane. Thus, the time at which the fluorescence intensity began to rapidly decrease ($t = 212$ s) corresponds to the time when pores were formed in the membrane.

On the other hand, a fluorescence microscope image of the GUV due to the fluorescence of CF-TP10 (Figure 2.3A (2)) shows that the fluorescence intensity of the rim of the GUV (the GUV membrane) gradually increased, and that by about 125 s it is essentially saturated (green squares in Figure 2.3B). This is despite the fact that the fluorescence intensity of the aqueous solution outside the GUV was low. These observations indicate that CF-TP10 binds rapidly to

the GUV membrane, and that the binding constant of CF-TP10 to the membrane is large.

The same experiments were carried out using 20 single GUVs. The gradual leakage of AF647 from a GUV started stochastically (Figure 2.3C), indicating that pores were formed stochastically. In all the examined GUVs, the fluorescence intensity of the GUV membrane became essentially saturated prior to pore formation. If we consider the irreversible two-state transition from the state of intact GUV (i.e., non-leaked GUV) to the state of GUV with pores (i.e., leaked GUV), we can obtain the rate constant of the two-state transition from the analysis of the time course of the fraction of intact GUVs, $P_{\mathrm{intact}}(t)$, among the population of GUVs examined, from which the fluorescent probe did not leak over time t. Here we define this rate constant as the rate constant of peptide-induced pore formation in lipid membranes (Tamba & Yamazaki, 2005; Tamba & Yamazaki, 2009; Tamba et al., 2010). Figure 2.3D shows that the value of P_{intact} of 20%DOPG/79%DOPC/1%biotin-lipid -GUVs decreased with time, and that the curve of the time course of P_{intact} was fit well by the single exponential decay function defined by eq. (2.1):

$$P_{\mathrm{intact}}(t) = \exp\left\{-k_{\mathrm{P}}(t - t_{\mathrm{eq}})\right\} \tag{2.1}$$

where k_{P} is the rate constant of CF-TP10-induced pore formation and t_{eq} is a fitting parameter denoting the time required for equilibrium binding of CF-TP10 to the GUV membrane. Three independent experiments similar to the experiment shown in Figure 2D were carried out to obtain the value for k_{P}. The average value of k_{P} was then calculated using the results of all the independent experiments. The average value of k_{P} for 1.9 μM CF-TP10 was 0.010 ± 0.001 s^{-1}, calculated from three independent experiments (N = 3).

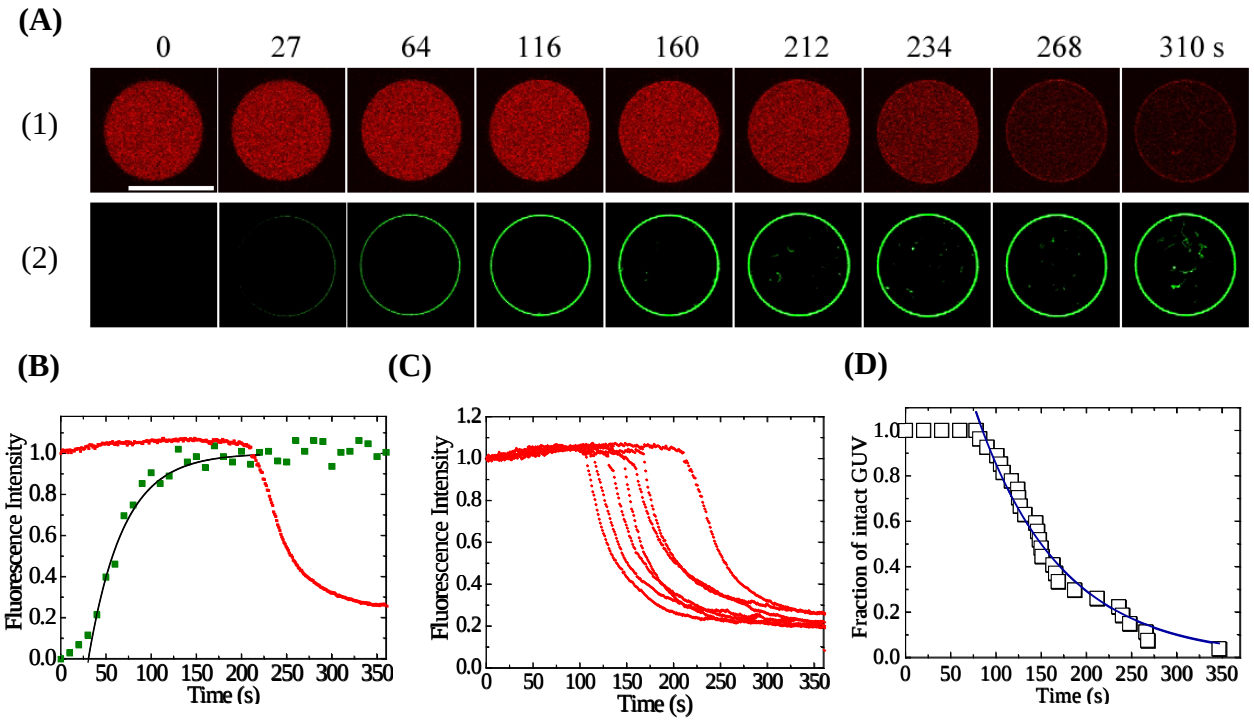

Figure-2.3: Leakage of AF647 and penetration of CF-TP10 in single 20%DOPG/79%DOPC/ 1%biotin-lipid-GUVs induced by 1.9 μM CF-TP10. (A) CLSM images of (1) AF647 and (2) CF-TP10. The numbers above each image show the time in seconds after CF-TP10 addition was started. The bar corresponds to 30 μm. (B) Time course of the change in normalized fluorescence intensity of the GUV shown in (A). Red and green points correspond to the fluorescence intensity of AF647 inside the GUV and of CF-TP10 in the rim of the GUV, respectively. The solid black line represents the best fit curve using eq. (2.7). The obtained value of k_{app} was 0.026 s^{-1}. (C) Other examples of the change in fluorescence intensity of AF647 inside single GUVs over time, using the same conditions as in (A). (D) Time course of P_{intact} of 20%DOPG/79%DOPC/1%biotin-lipid-GUV. The solid blue line represents the best fit curve using eq. (2.1). The obtained value of k_P was 0.011 s-1 and that of t_{eq} was 85 s.

We also investigated the rate constant of TP10-induced pore formation using the single GUV method and determined that it was 0.003 ± 0.001 s^{-1} for 1.9 μM TP10 (N = 3), which is smaller than the rate constant for CF-TP10. Figure 2.4 shows the dependence of the rate constant of CF-TP10 (or TP10)-induced pore formation on the concentration of CF-TP10 (or TP10), supporting the above result. The difference in rate constant is likely due to the binding constant of CF-TP10 with lipid membranes being larger than the binding constant of TP-10. Recently the same analysis using the time course of P_{intact} of single GUVs was successfully applied to the external tension-induced pore formation in a GUV to obtain its rate constant (Levadny et al., 2013).

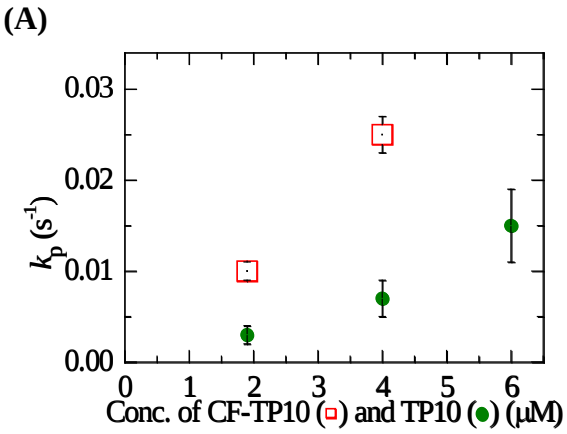

Figure-2.4: The dependence of the rate constant of CF-TP10 (or TP10)-induced pore formation in 20%DOPG/79%DOPC/1%biotin-lipid membranes on concentration. TP10 (●) and CF-TP10 (□). The rate constant of CF-TP10-induced pore formation was obtained by the analysis of the leakage of AF647 and that of TP10-induced pore formation was obtained by the analysis of leakage of calcein. The average values and standard errors of k_p were obtained.

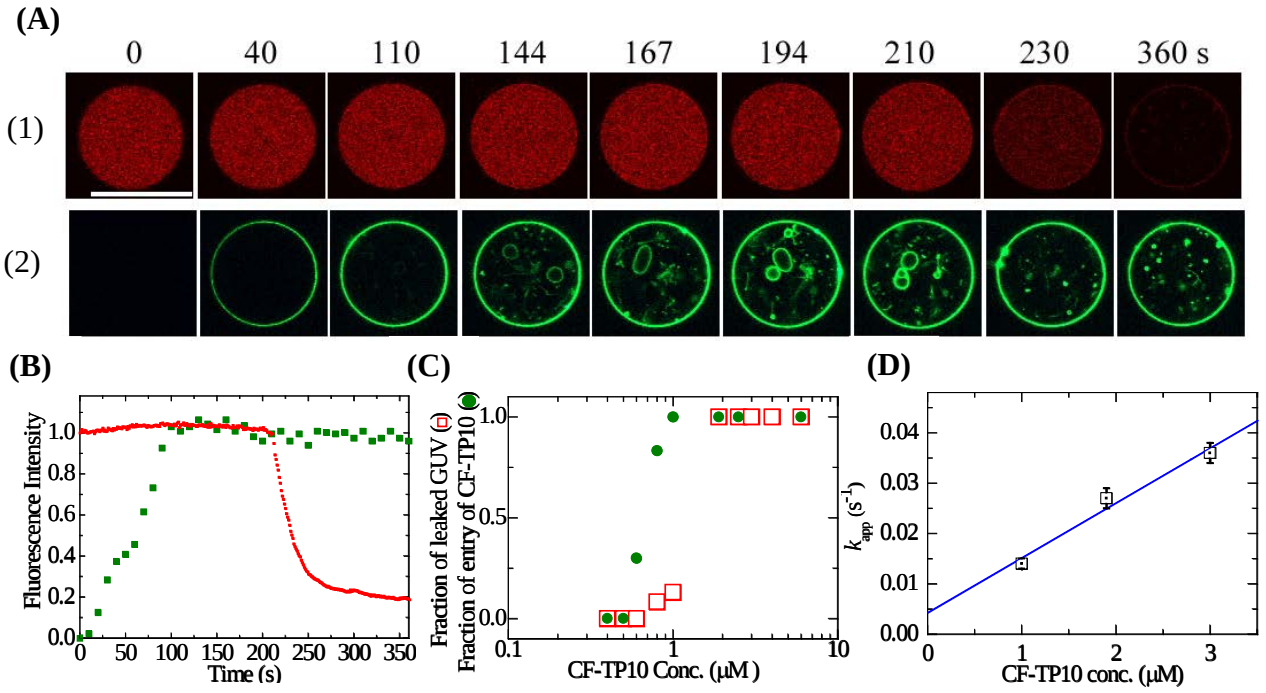

Figure-2.5: Leakage of AF647 and entry of CF-TP10 into single 20%DOPG/79%DOPC/ 1%biotin-lipid-GUVs containing smaller vesicles, induced by 1.9 μM CF-TP10. (A) CLSM images of (1) AF647 and (2) CF-TP10. The numbers above each image show the time in seconds after CF-TP10 addition was started. The bar corresponds to 30 μm. (B) Time course of the change in normalized fluorescence intensity of the GUV shown in (A). Red and green points correspond to the fluorescence intensity of AF647 inside the GUV and of CF-TP10 in the rim of the GUV, respectively. (C) Dependence of the fraction of entry of CF-TP10 before pore formation on the concentration of CF-TP10 (●). For comparison, the dependence of the fraction of leaked GUV after 6 min interaction on the concentration of CF-TP10 is shown (□). (D) Dependence of k_{app} on CF-TP10 concentration. The time course of the change in the fluorescence intensity of 15-25 GUVs with a diameter of 30-40 μm was measured. The average values and standard errors of k_{app} were obtained. The solid blue line represents the best fit curve using eq. (2.8).

To elucidate whether CF-TP10 enter the inside of a GUV under the experimental conditions of Figure 2.3, we used CLSM to investigate the interaction of CF-TP10 with single 20%DOPG/79%DOPC/1%biotin-lipid-GUVs containing smaller vesicles composed of 20%DOPG/80%DOPC and containing AF647. Figure 2.5A shows a typical experimental result of the effect of the interaction of 1.9 μM CF-TP10 with a single GUV. Figure 2.5A(1) and 2.5B show that CF-TP10 induced pores in the GUV membrane at 210 s, and then AF647 leaked through the pores rapidly. On the other hand, Figure 2.5A(2) shows that the fluorescence intensity of the GUV membrane gradually increased and at 100 s was almost saturated (green squares in Figure 2.5B). Some fluctuations of the intensity of the GUV membrane were caused by the smaller vesicles inside the GUV near the GUV membrane. At the beginning of the interaction, there was no fluorescence inside the GUV, but after 140 s, fluorescence intensity was observed due to the membranes of the smaller vesicles inside the GUV (t = 144, 167, and 194 s in Figure 2.5A(2)). This fluorescence occurred before CF-TP10-induced pore formation (210 s). These results indicate that CF-TP10 entered the inside of the GUV from the outside by translocating across the GUV membrane and then bound to the membrane of the smaller vesicles inside the GUV. The entry of CF-TP10 into the inside of the GUV occurred before pore formation. Next, we investigated the concentration dependence of the entry of CF-TP10 into a GUV before pore formation (i.e., before the leakage of AF647). Figure 2.6 shows the interaction of 1.0 μM CF-TP10 with single 20%DOPG/79%DOPC/1%biotin-lipid-GUVs containing smaller vesicles and AF647. The data indicate that CF-TP10 entered the inside of the GUV although pore formation did not occur before 6 min. At a CF-TP10 concentration of ≤1.0 μM, the probability of pore formation at 6 min was low (less than 0.2; Figure 2.5C), supporting the conclusion that CF-TP10 entered the intact GUV by translocating across the GUV membrane without pore formation. In the case of 0.8 μM CF-TP10, of the 12 GUVs examined, entry of CF-TP10 occurred before pore formation in 10 GUVs (i.e., fraction of entry of CF-TP10 = 0.83). Figure

2.5C shows the concentration dependence of the fraction of entry of CF-TP10. At and above 0.6 μM CF-TP10, the entry of CF-TP10 was observed in some examined GUVs, and the fraction of entry of CF-TP10 increased with an increase in CF-TP10 concentration and became 1.0 at and above 1.0 μM. These results clearly indicate that the translocation of CF-TP10 is a necessary condition, but not a sufficient condition, for the pore formation, i.e., some other factor determines the pore formation (see the detailed discussion later).

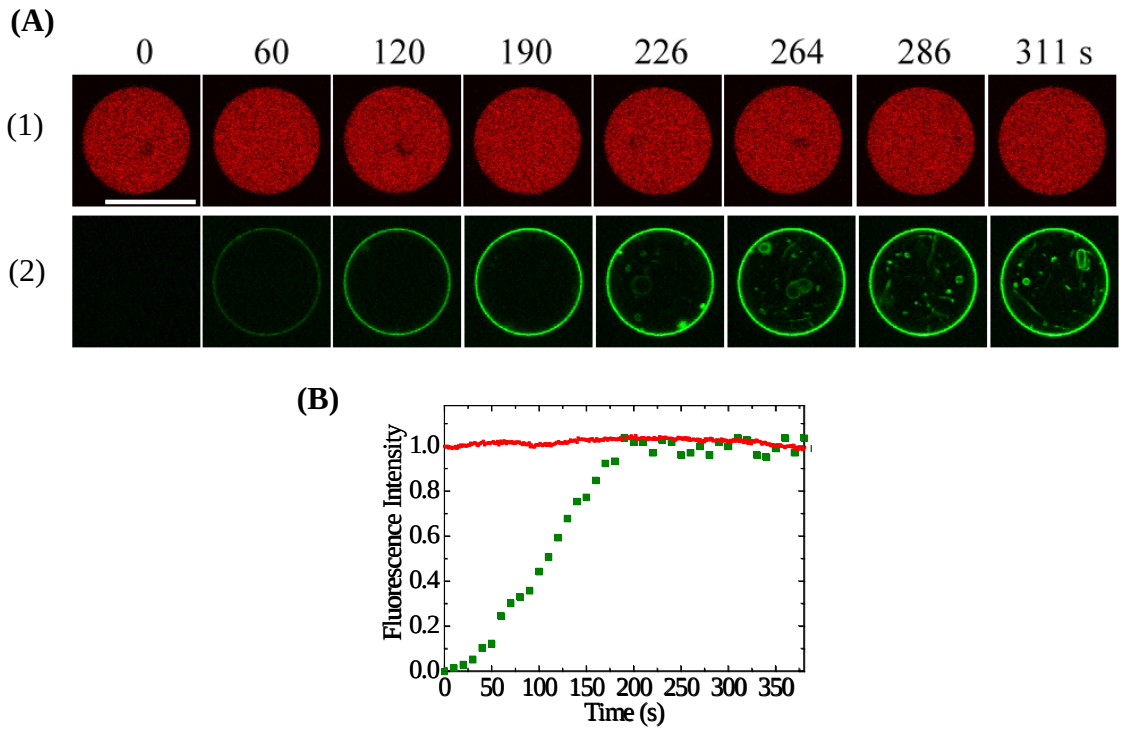

Figure-2.6: Leakage of AF647 and entry of CF-TP10 into single 20%DOPG/79%DOPC/ 1%biotin-lipid-GUVs containing smaller vesicles, induced by 1.0 μM CF-TP10. (A) CLSM images of (1) AF647 and (2) CF-TP10. The numbers above each image show the time in seconds after CF-TP10 addition was started. The bar corresponds to 30 μm. (B) Time course of the change in normalized fluorescence intensity of the GUV shown in (A). Red and green points correspond to the fluorescence intensity of AF647 inside the GUV and of CF-TP10 in the rim of the GUV, respectively.

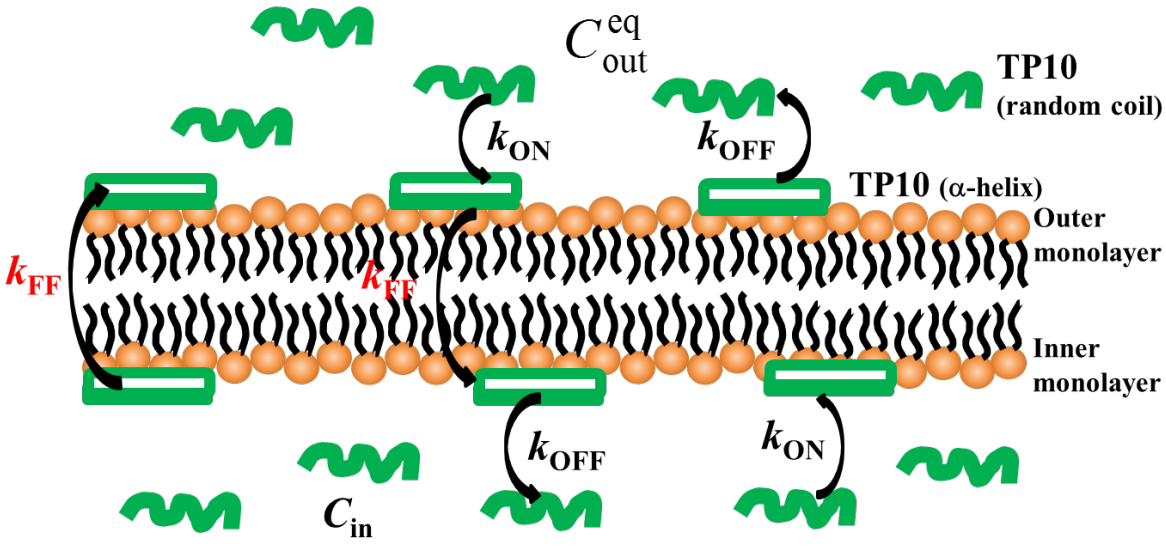

Figure-2.7: The scheme of entry of CF-TP10 through lipid bilayer membrane. TP10 in solution is random coil and its form α-helix structure when bind with lipid bilayer. k_{ON} and k_{OFF} are the rate constant of the binding and unbinding of TP10 with lipid membranes. k_{FF} the rate of transfer of TP10 from the outer to the inner monolayer or inner to the outer monolayer.

We next considered the kinetics of entry of CF-TP10 (Figure-2.7) and the time course of CF-TP10 concentration in the GUV membrane, $C_M(t)$ [M]. In the single GUV method, in the system considered there are only a single GUV and its surrounding aqueous solution at first. Then we add continuously a given concentration of CF-TP10 solution to the neighborhood of the single GUV by a micropipette until the end of observation of the GUV. Thereby the CF-TP10 concentration in aqueous solution near the GUV increased from zero to a constant equilibrium value, C_{out}^{eq} [M], for a short time and then it kept constant during the interaction of CF-TP10 with the single GUV, which was almost the same as that of the solution in the micropipette (Tamba & Yamazaki, 2009; Tanaka et al., 2004). This situation is almost the same as that of the surface plasmon resonance analysis (Gaidukov et al., 2003), but very different from that of the LUV suspension method where the peptide concentration in aqueous solution changes with time and greatly depends on lipid concentration. At the first step of the interaction, CF-TP10 binds at the membrane interface of the outer monolayer of the GUV. Since this surface area is limited, we can assume that there is the maximum concentration of the binding site of CF-TP10 at the membrane

interface of the monolayer, i.e., $C_{\mathrm{M}}^{\max}$ [M]. It is note that $C_{\mathrm{M}}^{\max}$ also has a physical meaning of the maximum concentration of the binding site of CF-TP10 at the membrane interface of the bilayer. Here we consider that one CF-TP10 molecule binds with one binding site, and thereby the CF-TP10 concentration in the monolayer is the same as the concentration of the occupied binding site of CF-TP10 at the membrane interface, and thereby $C_{\mathrm{M}}^{\max}$ is the maximum concentration of CF-TP10 in the monolayer and also in the bilayer. We further assume that the Langmuir binding isotherm holds here. θ_{OM} and θ_{IM} are the fraction of binding sites occupied by CF-TP10 in the outer and inner monolayer, respectively. Hence, the CF-TP10 concentration in the outer monolayer, C_{OM} [M], is $\theta_{\mathrm{OM}} C_{\mathrm{M}}^{\max}$, and the CF-TP10 concentration in the inner monolayer, C_{IM} [M] is $\theta_{\mathrm{IM}} C_{\mathrm{M}}^{\max}$. The rate of the binding of CF-TP10 with the outer monolayer of the GUV from aqueous solution is proportional to the concentration of unoccupied binding sites, $(1-\theta_{\mathrm{OM}}) C_{\mathrm{M}}^{\max}$, and the CF-TP 10 concentration in the aqueous solution outside the GUV, $C_{\mathrm{out}}^{\mathrm{eq}}$. Thus, the rate is equal to $k_{\mathrm{ON}} C_{\mathrm{out}}^{\mathrm{eq}} (1-\theta_{\mathrm{OM}}) C_{\mathrm{M}}^{\max}$, where k_{ON} is the rate constant of the binding. Next, the transfer of CF-TP10 from the outer to the inner monolayer occurs at a rate constant, k_{FF}. Finally, CF-TP10 transfers from the inner monolayer of the GUV into the aqueous solution inside the GUV at a rate constant of k_{OFF}. We also have to consider backward reactions. Thereby, C_{OM}, C_{IM}, and the CF-TP10 concentration in the aqueous solution inside the GUV, C_{in}, can be expressed by the following differential equations.

$$\frac{dC_{\mathrm{OM}}}{dt} = k_{\mathrm{ON}} C_{\mathrm{out}}^{\mathrm{eq}} (1-\theta_{\mathrm{OM}}) C_{\mathrm{M}}^{\max} - k_{\mathrm{FF}} \theta_{\mathrm{OM}} C_{\mathrm{M}}^{\max} + k_{\mathrm{FF}} \theta_{\mathrm{IM}} C_{\mathrm{M}}^{\max} - k_{\mathrm{OFF}} \theta_{\mathrm{OM}} C_{\mathrm{M}}^{\max} \tag{2.2}$$

$$\frac{dC_{\mathrm{IM}}}{dt} = k_{\mathrm{FF}} \theta_{\mathrm{OM}} C_{\mathrm{M}}^{\max} - k_{\mathrm{FF}} \theta_{\mathrm{IM}} C_{\mathrm{M}}^{\max} - k_{\mathrm{OFF}} \theta_{\mathrm{IM}} C_{\mathrm{M}}^{\max} + k_{\mathrm{ON}} C_{\mathrm{in}} (1-\theta_{\mathrm{IM}}) C_{\mathrm{M}}^{\max} \tag{2.3}$$

$$\frac{dC_{\mathrm{in}}}{dt} = k_{\mathrm{OFF}} \theta_{\mathrm{IM}} C_{\mathrm{M}}^{\max} - k_{\mathrm{ON}} C_{\mathrm{in}} (1-\theta_{\mathrm{IM}}) C_{\mathrm{M}}^{\max} \tag{2.4}$$

Initially, C_{in} is very low and so the term $k_{\mathrm{ON}} C_{\mathrm{in}} (1-\theta_{\mathrm{IM}}) C_{\mathrm{M}}^{\max}$ can be neglected. We can obtain the time derivative of the average concentration of CF-TP10 in the GUV bilayer, C_{M},

using eqs. (22), (2.3), and $C_M = (C_{OM} + C_{IM})/2$.

$$\begin{aligned}\frac{dC_M}{dt} &= \frac{1}{2}\{k_{ON}C_{out}^{eq}(1-\theta_{OM})C_M^{max} - k_{OFF}\theta_{OM}C_M^{max} - k_{OFF}\theta_{IM}C_M^{max}\} \\ &= \frac{1}{2}\{k_{ON}C_{out}^{eq}C_M^{max} - k_{ON}C_{out}^{eq}C_{OM} - k_{OFF}C_{OM} - k_{OFF}C_{IM}\}\end{aligned} \tag{2.5}$$

Generally it is difficult to obtain $C_M(t)$ due to some unknown parameters. If the transfer of CF-TP10 between the outer and inner monolayers is fast, i.e., the rate of the transfer is larger than that of the binding of CF-TP10 and that of its transfer from the membrane to aqueous solution (i.e., $k_{FF} >> k_{ON}C_{out}^{eq}$, and $k_{FF} >> k_{OFF}$), we can approximate that $C_{OM} \approx C_{IM} \approx C_M$. Under this condition, eq. (2.5) can be converted to eq. (2.6):

$$\frac{dC_M}{dt} = \frac{1}{2}k_{ON}C_{out}^{eq}C_M^{max} - (\frac{1}{2}k_{ON}C_{out}^{eq} + k_{OFF})C_M \tag{2.6}$$

The solution of this differential equation (2.6) under the initial condition ($C_M(0) = 0$) becomes

$$C_M(t) = \frac{C_M^{max}}{1+\frac{2}{K_B C_{out}^{eq}}}\left[1-\exp\{-\left(\frac{1}{2}k_{ON}C_{out}^{eq} + k_{OFF}\right)t\}\right] \tag{2.7}$$

$$= A\,[1-\exp(-k_{app}t)]$$

$$\text{where} \quad k_{app} = k_{ON}C_{out}^{eq}/2 + k_{OFF} \tag{2.8}$$

where $K_B = k_{ON}/k_{OFF}$ is the binding constant of CF-TP10 to the lipid membrane and k_{app} is the apparent rate constant of the increase in CF-TP10 concentration in the GUV membrane, $C_M(t)$. The time course of the fluorescence intensity of the rim of the GUV (Figure 2.3B) was fit well by eq. (2.7) (the black line in Figure 2.3B), which gave a value for the rate constant k_{app} of 0.026 s^{-1}. We also obtained the dependence of k_{app} on CF-TP10 concentration. As expected from eq. (2.8), k_{app} increased linearly with an increase in CF-TP10 concentration, C_{out}^{eq}. Fitting the data to eq. (2.8) in Figure 2.5D provided values for k_{ON} and k_{OFF}: $k_{ON} = 2.2 \times 10^4\ M^{-1}s^{-1}$ and $k_{OFF} = 4.2 \times 10^{-3}\ s^{-1}$ (i.e., $K_B = 5.2 \times 10^6\ M^{-1}$). Since CF-TP10 contains a hydrophobic fluorescent probe, CF, K_B of CF-TP10 may be larger than that of TP10. However, we don't have other experimental

evidence that the transfer of CF-TP10 between outer and inner monolayers is fast, and hence we need further studies.

We also investigated the interaction of CF-TP10 with single DOPC-GUVs containing AF647 and smaller vesicles inside the GUVs using CLSM. We obtained essentially identical results as for 20%DOPG/79%DOPC/1%biotin-lipid-GUVs, although a lower concentration of CF-TP10 induced leakage of AF647 and translocation of CF-TP10 across the lipid membrane into single GUVs prior to pore formation.

The above results indicate that CF-TP10 can transfer from the outer to the inner monolayer before pore formation. The concentration imbalance of CF-TP10 between the outer and the inner monolayer induces strain in the lipid membrane, which may be one of the factors of the transfer (Yandek et al., 2007). Such transfer of CF-TP10 would perturb the structure of lipid membranes, which might induce a transient leakage of small molecules such as ions. Molecular dynamics simulations indicate that some amphipathic peptides can transfer from the outer to the inner monolayer (Lopez et al., 2006; Leontiadou et al., 2006). However, the mechanism of this transfer is not completely clear from biophysical point of view at present, and thereby further studies are indispensable.

2.3.2 The size of TP10-induced pores in the lipid membranes of GUVs:

In order to examine the size of the TP10-induced pores in lipid membranes, we investigated the leakage of a water-soluble fluorescent probe, TRD-40k, using phase contrast fluorescence microscopy. The molecular weight distribution of TRD-40k is 35,000–50,000 according to the manufacturer, and its Stokes-Einstein radius, $R_{SE,}$ is 5.0 nm (Tamba et al., 2010). Figure 2.8A shows the effect of the interaction of 6.0 μM TP10 with single 20%DOPG/79%DOPC/1%biotin-lipid-GUVs containing TRD-40k. Prior to TP10 addition, a phase contrast microscope image of the GUV showed high contrast (Figure 2.8A-1) due to the

difference in the concentration of sucrose and glucose between the inside (0.1 M sucrose) and the outside (0.1 M glucose) of the GUV. A fluorescence microscope image of the same GUV (Figure 2.8A-2) showed a high concentration of TRD-40k inside the GUV at this time. During addition of a 6.0 μM solution of TP10, the fluorescence intensity inside the GUV remained similar over the first 52 s, followed by a gradual decrease in fluorescence intensity (Figure 2.8A-2, 2.8C). After 360 s, less than 10% of the original fluorescence intensity was detected inside the GUV. The time course of this decrease in fluorescence intensity of the inside of the GUVs due to TRD-40k was fit well by a single exponential decay curve (Figure 2.8C). A comparison of the phase contrast images in Figure 2.8A-1 and 2.8A-3 also shows a substantial loss in the phase contrast of the GUV, indicating that leakage of TRD-40k was accompanied by passage of sucrose and glucose through the same pore. The images also show that the diameter of the GUV decreased by 16%, and the presence of a few small, high-contrast particles on the membrane of the GUV. These data indicate that TRD-40k can pass through TP10-induced pores in the GUV membrane. When the same experiments were carried out using 25 single GUV, similar leakage of TRD-40k from a GUV started stochastically. Figure 2.8E shows that the value of P_{intact} of 20%DOPG/79%DOPC/1%biotin-lipid-GUVs containing TRD-40k decreased with time, and that the curve of the time course of P_{intact} was fit well by the single exponential decay function defined by eq. (2.1). The average value of k_P for 6.0 μM TP10 was 0.010 ± 0.001 s^{-1} and the average value of t_{eq} was 53 ± 13 s, calculated from four independent experiments similar to Figure 2.8E (N = 4). This k_P value is a little smaller than that obtained using 20%DOPG/79%DOPC/1%biotin-lipid-GUVs containing calcein. In 50% of the GUVs examined, the diameter of the GUV did not change, but in the other 50% the diameter decreased by 10-20%. In some GUVs, the multi-step of the decrease in the fluorescence intensity of the GUV was observed. Similar results were obtained for the TP10-induced leakage of TRD-10k (Figure 2.8B, D, F). The average value of k_P for 4.0 μM TP10 was 0.005 ± 0.001 s^{-1} and the average value of

t_{eq} was 190 ± 40 s (N = 3). At present we don't know the reason why the rate constants of the TP10-induced pore formation in the GUVs containing TRD-40k is a little smaller than those in the GUVs containing calcein. There may be some interactions between TP10 and TRD-40k inside the GUVs.

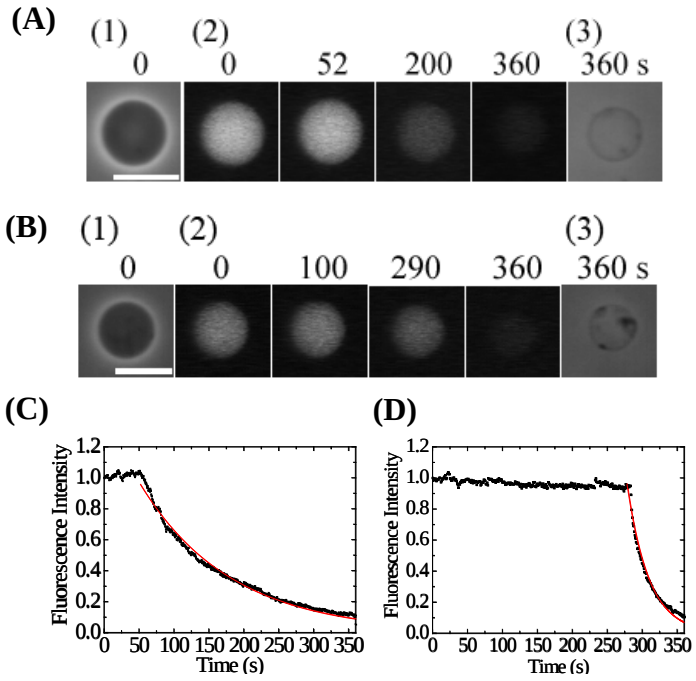

Figure-2.8: The size of TP10-induced pores in 20%DOPG/79%DOPC/1%biotin-lipid-GUVs. (A)(C) Leakage of TRD-40k from single 20%DOPG/79%DOPC/1%biotin-lipid-GUVs induced by 6 μM TP10 in buffer H at 25 °C. (A) Fluorescence images (2) show that the TRD-40k concentration inside the GUV progressively decreased after the addition of TP10. The numbers above each image show the time in seconds after TP10 addition was started. Also shown are phase contrast images of the GUV at time 0 (1) and 360 s (3). The bar corresponds to 20 μm. (C) Time course of the change in the normalized fluorescence intensity of the GUV shown in (A). The solid red line represents the best fit curve using a single exponential decay function. (B)(D) Leakage of TRD-10k from single 20%DOPG/79%DOPC/ 1%biotin-lipid-GUVs induced by 4 μM TP10 in buffer H at 25 °C. (B) Fluorescence images (2) show that the TRD-10k concentration inside the GUV progressively decreased after the addition of TP10. The numbers above each image show the time in seconds after TP10 addition was started. Also shown are phase contrast images of the GUV at time 0 (1) and 360 s (3). The bar corresponds to 20 μm. (D) Time course of the change in the normalized fluorescence intensity of the GUV shown in (B). The solid red line represents the best fit curve using a single exponential decay function.

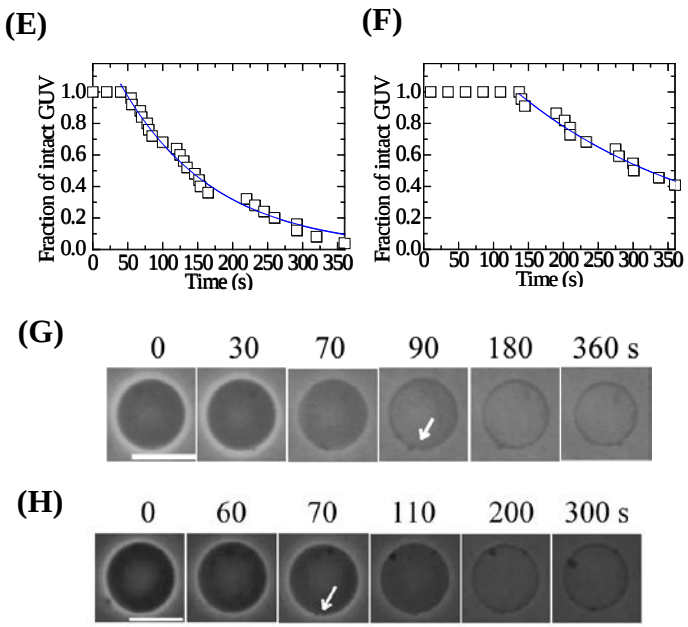

Figure-2.8(contd.): (E) Time course of P_{intact} of 20%DOPG/79%DOPC/1%biotin-lipid-GUV containing TRD-40k in the presence of 6 μM TP10 in buffer H at 25 °C. The solid blue line represents the best fit curve using eq. (2.1). The obtained value of k_P was 0.008 s^{-1}. (F) Time course of P_{intact} of 20%DOPG/79%DOPC/1%biotin-lipid-GUV containing TRD-10k in the presence of 4 μM TP10 in buffer H at 25 °C. The solid blue line represents the best fit curve using eq. (2.1). The obtained value of k_P was 0.004 s^{-1}. (G) Leakage of sucrose from single 20%DOPG/79%DOPC/1%biotin-lipid-GUVs induced by 6 μM TP10. Phase contrast images are shown. A white arrow shows a local rupture of the membrane. The bar corresponds to 20 μm. (H) Leakage of sucrose from single 20%DOPG/79%DOPC/1%biotin-lipid-GUVs containing TRD-40k induced by 6 μM TP10. Phase contrast images are shown. A white arrow shows a local rupture of the membrane. The bar corresponds to 20 μm.

To understand the mechanism underlying the decrease in GUV diameter, the interaction of TP10 with single 20%DOPG/79%DOPC/1%biotin-lipid-GUVs containing 0.1 M sucrose and no TRD-40k was investigated using phase contrast microscopy. Figure 2.8G shows that after single-site rupture of the GUV membrane (shown by a white arrow), the GUV diameter gradually decreased. However, the local rupture did not always decrease the diameter of GUVs. Similar results were obtained for the interaction of TP10 with single 20%DOPG/ 79%DOPC/1%biotin-lipid-GUVs containing TRD-40k (Figure 2.8H). On the basis of these results, large molecules such as TRD-40k and TRD-10k can permeate through a TP10-induced pore or the TP10-induced local rupture of the membrane. The mechanism of the TP10-induced rupture of the membrane and the resultant decrease in diameter of the GUV remains unknown, although a similar decrease in the diameter of a GUV was observed in the interaction of mastoparan with a GUV (Dos Santos Cabrera et al., 2011).

On occasion, a smaller vesicle inside a GUV exited through the TP10-induced pore or the local rupture. Figure 2.9 shows an example of the exit of a smaller vesicle with a diameter of 1-2 μm from the mother GUV in the interaction of 2.5 μM CF-TP10 with a 20%DOPG/79%DOPC/1%biotin-lipid- GUV. At 97.6 s a few small vesicles were observed near the membrane inside the mother GUV, and from 98.8 s to 99.9 s they have exited the mother GUV.

The results clearly show that large molecules such as TRD-40K and vesicles with a diameter of 1-2 μm can translocate across the lipid bilayer. This is the first direct experimental evidence that TP10 can deliver large cargo through lipid membranes. The mechanism of these TP10-induced pore formation and local rupture is not clear at present.

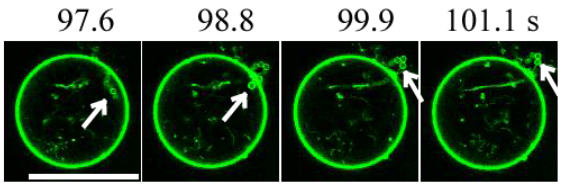

Figure-2.9: Exit of small vesicles with a diameter of 1-2 μm from the inside of a GUV induced by 2.5 μM CF-TP10. Experimental conditions are the same as for Figure 2.3. A white arrow shows smaller vesicles which exited from the mother GUV. The bar corresponds to 40 μm.

2.3.3 The translocation of peptides across lipid membrane and the peptide-induced pore formation:

As shown in the kinetics of the concentration of CF-TP10 in the GUV membrane, the translocation of CF-TP10 across the lipid membranes (i.e., the transfer of CF-TP10 from the outer to the inner monolayer) occurs continuously, indicating that the activation energy of the translocation is low. In contrast, CF-TP10 (or TP10) induced pore formation in lipid membranes stochastically, indicating that the activation energy of the pore formation is large. Moreover, the results in this thesis clearly indicate that CF-TP10 translocates across the lipid membranes at an early stage and then in a subsequent stage the pore formation occurs in the lipid membranes (i.e., the pore formation occurs after the translocation of peptides). At low concentrations of CF-TP10 (from 0.6 to 1 μM) the translocation of CF-TP10 did not induce the pore formation in most GUVs (Figure 2.5C). These results indicate that the translocation of CF-TP10 is a necessary condition, but not a sufficient condition, for the pore formation, i.e., some other factor determines the pore formation. The translocation of CF-TP10 increases the concentration of CF-TP10 in the inner monolayer, and the kinetic analysis suggests that the concentrations of CF-TP10 in both the monolayer are similar. The $C_{\mathrm{M}}^{\max}$ value increases with an increase in CF-TP10 concentration in a buffer, and thereby we can consider reasonably that the CF-TP10 concentration in both the monolayer plays an important role in the pore formation. This characteristic is similar to that of the pore formation induced by melittin, a bee venom peptide with a lytic activity against eukaryote cells (Lee et al., 2013). It is important to note that the pore formation took a long time after the CF-TP10 concentration in the membrane became a maximum, steady value, $C_{\mathrm{M}}^{\max}$ (e.g., Figure 2.3B and Figure 2.5B), which is different from the case of melittin.

In contrast, as for antimicrobial peptide, magainin 2, we have proposed the different scheme of pore formation as follows. Magainin 2 molecules locate in the membrane interface of

only the outer monolayer before pore formation, which induces a stretching of the inner monolayer. We consider that this stretching plays an important role in pore formation. The data of the magainin 2-induced leakage of TRD-10k and TRD-40k from single GUVs show the transient, rapid leakage in the initial stage followed by a stage of slow leakage, indicating that magainin 2 molecules initially induce a transient, large pore in lipid membranes following which the radius of pore decreases to a stable smaller size (Tamba et al., 2010). It is also reported that the α5 segment from the proapoptotic protein Bax (Baxα5) induced pores in lipid membranes and the size of this pore is large at the initial stage and then decreased to a smaller, equilibrium one with time (Fuertes et al., 2010). As shown in Figure 2.8, most of the time courses of TP10-induced leakage of TRD-10k and TRD-40k from single GUVs were fit well by single exponential decay curves, indicating that the size of the TP10-induced pore does not change with time. This result is different from that of magainin 2 and Baxα5 peptides. To confirm our hypothesis on the magainin 2-induced pore, we need the experimental evidence of the location of magainin 2 in a single GUV before pore formation, which can be obtained using the same method in this thesis.

2.3.4 Advantage of the single GUV method:

We succeed in obtaining new information on the interaction of TP10 with lipid membranes using the single GUV method. We separated the elementary processes of TP10-induced leakage of fluorescent probe (i.e., TP10-induced pore formation in lipid membranes and leakage of fluorescent probe through the pores), and succeed in determining the rate constant of TP10-induced pore formation. We obtained the time course of the CF-TP10 concentration in the membrane, and its relationship with the entry of CF-TP10 into the inside of GUVs. The simultaneous experiment of the leakage of the fluorescent probe and the entry of CF-TP10 clearly shows that CF-TP10 translocates across the lipid membrane before pore

formation. These results cannot be obtained using the LUV suspension method.

A paper on the translocation of cationic amphipathic peptides across the GUV membrane was published (Wheaten et al., 2013). The experimental method used in their paper (here we call it the GUV suspension method) is different from the single GUV method used in this thesis; in the GUV suspension method many GUVs were suspended in a solution of a water-soluble fluorescent probe, carboxyfluorescein (CF), and Lissamine Rhodamine B (Rh) labeled peptides (TP10W and DL1a). The GUVs contained smaller inner GUVs. First CF and peptides entered the inside of the outer GUV, and then the translocation of peptides into the inside of the inner GUVs and influx of CF into the inner GUVs occurred. The authors observed that the translocation of peptide into the inner GUVs occurred gradually and the influx of CF into the inner GUVs rapidly. However, in their paper there are no quantitative results such as peptide concentration dependence of the translocation of peptides and the rate constant of the peptide-induced pore formation. The rate of the translocation of peptides across the inner GUV membrane in their paper (characteristic time is 10 min) was very low compared with that of CF-TP10 in our thesis, although it is difficult to compare the rate because the equilibrium concentration of peptide is unknown in their paper. Irrespective of these differences in the experimental data and method, their results support the conclusion in this thesis qualitatively.

The advantage of the single GUV method over their GUV suspension method is as follows. (1) In the single GUV method, we can control the concentration of peptides outside a single GUV (i.e., $C_{\mathrm{out}}^{\mathrm{eq}}$), and thereby we can obtain detailed information on peptide concentration dependence of the translocation of peptides and the peptide-induced pore formation (e.g., Figure 2.4, Figure 2.5C and 2.5D). In contrast, in the GUV suspension method, many GUVs are added in a given concentration of peptide solution, and hence the peptide concentration outside the GUV depends on GUV concentration (i.e., lipid concentration) in the suspension, which cannot be controlled well, and it also changes with time because the binding of peptides with GUV

membranes and the entry of peptides into the inside of the GUVs increase with time. This is the same situation of the LUV suspension method. On the other hand, in the single GUV method, we cannot determine the peptide to lipid molar ratio in the system, which is determined in the LUV suspension method and the GUV suspension method. (2) In the single GUV method it is easier to carry out many experiments using a single GUV and analyze these results statistically to obtain the rate constants of the elementary steps. (3) In the single GUV method, we can follow rapid reaction of peptide translocation and pore formation because we can observe the GUV from the start of the interaction of peptides with the GUV (i.e., $t = 0$). On the other hand, the advantage of the GUV suspension method is that no special apparatus and experimental technique such as handling of micropipette are required. However, it is evident that both the single GUV method and the GUV suspension method are superior to the LUV suspension method, and hence these methods will become powerful methods to reveal the interaction of peptides such as CPPs with lipid membranes.

From the results in this thesis, we should learn an important lesson for investigation of translocation of peptides such as CPPs across the lipid membranes. Some peptides such as TP10 and magainin 2 (Tamba et al, 2010) induce a pore which size is larger than that of the peptide. In this case after the pore formation peptides can easily enter the inside of vesicles by diffusion through the pore, and thereby the increase in the peptide concentration inside the GUV or at the membranes of smaller vesicles inside the GUV does not indicate the translocation of peptide across the membrane. Only when the transfer of peptides into the inside of GUVs occurs before pore formation or the size of the peptide-induced pore is smaller than that of the peptide, the increase in the peptide concentration inside the GUV corresponds to the translocation of peptide across the membrane. Thereby to study the translocation of peptides, the simultaneous measurement of the peptide-induced pore formation and the transfer of peptides into the inside of GUVs is indispensable (Boll et al, 2011).

2.3.5 Biological implications:

In this thesis we clearly show that TP10 translocates across the lipid membranes and subsequently the pore formation occurs in the membrane. The size of the pore is so large that TRD-40K and vesicles with a diameter of 1-2 μm can pass through the pore. This provides experimental evidence to explain why TP10 can deliver large cargo through plasma membranes without the need for special transport mechanisms such as those found in cells. Based on the results in this thesis, we can reasonably consider that if TP10 could dissociate from its cargo at or near the plasma membranes the yield of cellular uptake of cargo would increase because the translocation of TP10 is expected to be faster than that of TP10 connected with a hydrophilic cargo such as oligonucleotide and protein. The experimental results of TP10-induced cellular uptake of decoy oligonucleotide targeting the Myc protein may support the above hypothesis; the yield of cellular uptake of a non-covalent electrostatic complex of TP10 with Myc decoy (i.e., the TP10-Myc decoy complex) is much larger than that of a complex of TP10 which is covalently attached with peptide nucleic acid with TP10 (E.L.–Andaloussi et al., 2005). However, we do not know whether a complex of TP10 covalently attached to proteins and oligonucleotides can induce pore formation and translocate across lipid membranes. To validate our hypothesis and address the above question, it is important to investigate effects of cargo molecules and the kinds of the attachment of cargo with TP10 on the TP10-induced translocation of cargo molecule across lipid membranes.

2.4 CONCLUSION:

The results in this thesis show that CF-TP10 translocated continuously across the lipid membrane of a single GUV before pore formation (i.e., without leakage of fluorescent probes) and then subsequently pore formation occurred in lipid membranes. Moreover, at a lower concentration of CF-TP10, pore formation did not occur after the translocation of CF-TP10, indicating that some other factor is necessary for pore formation. We measured the time course of CF-TP10 concentration at the GUV membrane, which was fit well by a theoretical equation based on a model for CF-TP10 translocation across the GUV membrane. After the translocation of CF-TP10 completed, the pores were formed in the GUV membranes stochastically. We determined the rate constant of CF-TP10-induced pore formation, which increased with an increase in CF-TP10 concentration. These results clearly show that translocation of CF-TP10 into the GUVs and CF-TP10-induced pore formation are different phenomena, and that the former occurs in the absence of the latter. We also investigated the size of the TP10-induced pore in lipid membranes and found that large molecules such as TRD-40K, and vesicles with a diameter of 1-2 μm, translocate across the lipid bilayer. This result indicates that large molecules can pass through the TP10-induced pores in lipid membranes. As discussed in the Introduction, TP and TP10 can deliver a large protein such as an antibody, oligonucleotide, and colloidal gold (diameter 10 nm) as cargo (Pooga et al., 2001; E.L.-Andaloussi et al., 2005), but the mechanism is poorly understood. Our results directly indicate that TP10 can deliver large proteins and gold particles as cargo through the TP10-induced pores in the lipid membrane without the need for special mechanisms found in cells. In the conclusion, the results in this thesis revealed the elementary steps of entry of TP10 into a single vesicle and TP10-induced pore formation in the membrane, and the new experimental methods in this thesis will be used to reveal the mechanism of these phenomena and to design new CPPs and antimicrobial peptides.

Chapter-3

Effects of cholesterol on the entry of cell-penetrating peptide transportan 10 into a single vesicle and TP10-induced pore formation.

3.1 INTRODUCTION:

As described in chapter 2, TP10 has an ability to translocate across the lipid membrane and enter into single 20%DOPG/80%DOPC-GUVs or 100%DOPC-GUVs before TP10-induced pore formation. It is reported that the TP and its truncated analogue TP10 can translocate across the plasma membrane and enter cells within very short time (Padari et al., 2005). On the other hand, plasma membranes of eukaryote cells contains high concentrations of cholesterol (Yeagle, 1985; Bloom & Mouritsen, 1995). High concentrations of cholesterol affect various physical properties of lipid membranes such as an increase in the elastic area compressibility modulus (Needham & Nunn, 1990), lipid ordering and diffusion coefficient of lipid molecules (Yeagle, 1985).

The effects of cholesterol (chol) on the interaction of TP10 or TP with lipid membrane have not been sufficiently investigated. The interactions of Cys-TP (a TP analogue with replacement of Lys in TP10 with Cys) with dimyristoylphosphatidylcholine (DMPC) and DMPC/chol membrane were examined, Cys-TP caused lipid ordering and a large increase in membrane permeation in pure DMPC-membrane and DMPC membrane containing low concentration of cholesterol. In contrast, for DMPC/chol membrane in the liquid-ordered (lo) phase, the lipid ordering and increase in membrane permeation were not induced by Cys-TP10. (Arsov et al., 2008). However no research on the effect of cholesterol on entry of TP or TP10 into a single vesicle.

To elucidate the mechanism of the entry of TP10 into cells, it is important to investigate the effect of cholesterol on the entry of TP10 into a single vesicle and on the interaction of TP10

with lipid membranes. In this chapter, we investigate the effects of cholesterol on the entry of TP10 into a GUV and its pore formation using the single GUV method.

3.2 MATERIALS AND METHODS:

3.2.1 Materials:

DOPC and DOPG were purchased from Avanti Polar Lipids Inc. (Alabaster, AL). Bovine serum albumin (BSA) was purchased from Wako Pure Chemical Industry Ltd. (Osaka, Japan). Cholesterol, biotin-labeled BSA and streptavidin were purchased from Sigma-Aldrich Co. (St. Louis, MO, USA). AF647, 5-(and 6)-carboxyfluorescein succinimidylester, and N-((6-(biotinoyl)amino)-hexanoyl)-1,2-dihexadecanoyl-*sn*-glycero-3-phosphoethanolamine, triethyl ammonium salt (biotin-X-DHPE, referred to as biotin-lipid) were purchased from Invitrogen Inc. (Carlsbad, CA). Calcein was purchased from Dojindo Laboratory (Kumamoto, Japan). TP10 was synthesized by the FastMoc method using a 433A peptide synthesizer (PE Applied Biosystems, Foster City, CA). The fluorescence probe carboxyfluorescein-labeled TP10 (CF-TP10), which has one fluorophore CF at the N-terminus of the peptide, was synthesized using a standard method by the reaction of 5-(and 6)-carboxyfluorescein succinimidylester with TP10-peptide resin (Chapter 2). The methods for TP10 and CF-TP10 cleavages from the resin, purification and identification of these peptides were described previously.

3.2.2 Production and purification of GUVs:

GUVs of DOPG/DOPC/chol/biotin-lipid (molar ratio: 20/59/40/1, whose cholesterol concentration is 33 mol% and surface charge density is almost the same as 20%DOPG/80%DOPC membrane) were prepared by incubation of buffer H (10 mM HEPES, pH 7.5, 100 mM NaCl, and 1 mM EGTA) containing 0.1 M sucrose and various fluorescent probes with dry lipid films by the natural swelling at 37 °C. To prepare GUVs containing smaller

vesicles, a GUV (80%DOPC/20%DOPG) suspension was prepared in a buffer containing no fluorescent probes using the above method, then the GUV suspension was centrifuged to remove multilamellar vesicles and lipid aggregates. A mixture of the partially purified GUV suspension and AF647 solution in buffer H containing 0.1 M sucrose was incubated with dry lipid films at 37 °C. The membrane filtering method was used to remove untrapped fluorescent probes (Tamba et al., 2011).

3.2.3 Experiments using single GUV method:

Purified GUV suspension (300 μL: 0.1M sucrose in buffer H as the internal solution; 0.1M glucose in buffer H as the external solution) was transferred into a hand-made microchamber (Chapter 2). Single GUVs were fixed on a slide glass or a coverslip in the chamber using the strong association between biotin and streptavidin (Chapter 2). The GUVs were observed using a CLSM (FV-1000, Olympus, Tokyo, Japan) or an inverted fluorescence phase contrast microscope (IX-70, Olympus) at 25±1 °C using a stage thermocontrol system (Thermoplate, Tokai Hit, Shizuoka, Japan). For measurements using IX-70, phase contrast and fluorescence images of GUVs were recorded using a high-sensitivity fluorescence camera (EM-CCD camera, C9100-12, Hamamatsu Photonics K.K., Hamamatsu, Japan) containing a hard disk. The fluorescence intensity inside the GUVs was determined using an AquaCosmos (Hamamatsu Photonics K.K.) and the average intensity per GUV was estimated. During the interaction of peptides with a single GUV, various concentrations of CF-TP10 or TP10 in buffer H containing 0.1 M glucose were added continuously to the vicinity of the GUV through a 20-μm-diameter glass micropipette positioned by a micromanipulator. The distance between the GUV and the tip of the micropipette was ~60 μm. The details of this method were described in chapter 2. Obtaining the time course of the fluorescence intensity of the rim and inside of the GUV as a function of time during the interaction of CF-TP10 (or TP10), we used special

methodology. The details of this method were described previously (Chapter 2).

3.3 RESULTS AND DISCUSSION:

3.3.1. Effects of cholesterol on the entry of TP10 into single vesicles:

We investigated the effects of cholesterol on the entry of CF-TP10 into a GUV and the CF-TP10-induced pore formation in lipid membranes. For this purpose, we used GUVs of DOPG/DOPC/chol/biotin-lipid (20/59/40/1, molar ratio). These GUVs contained smaller vesicles composed of 20%DOPG/80%DOPC and AF647. Figure 3.1A shows a typical experimental result of the effect of the interaction of 2.0 μM CF-TP10 with a single GUV. The CF-TP10 solution was continuously provided to the GUV surroundings through a micropipette. A fluorescence microscope image of the GUV (Figure 3.1A (1)) shows a high concentration of AF647 inside the GUV. During the addition of the 2.0 μM solution of CF-TP10, the fluorescence intensity inside the GUV remained essentially constant. This result shows that no leakage of AF647 occurred during the interaction of CF-TP10 with the GUV, indicating that no pore formation occurred in the GUV membrane. Figure 3.1B and 3.1A (2) shows that the fluorescence intensity of the GUV membrane gradually increased and at 70 s was almost saturated. On the other hand, at the beginning of the interaction, there was no fluorescence due to smaller vesicles inside the GUV, but after 340 s, fluorescence intensity was observed due to the membranes of the smaller vesicles inside the GUV (Figure 3.1A(2)), and this fluorescence occurred without CF-TP10-induced pore formation. Thereby, Figure 3.1A and B show that CF-TP10 entered the GUV although pore formation did not occur before 375 s. Figure 3.1C shows the concentration dependence of the fraction of entry of CF-TP10 before pore formation of GUVs. At and above 2.0 μM CF-TP10, the entry of CF-TP10 was observed in some examined GUVs, and the fraction of entry of CF-TP10 increased with an increase in CF-TP10 concentration and became 1.0 at 4.0

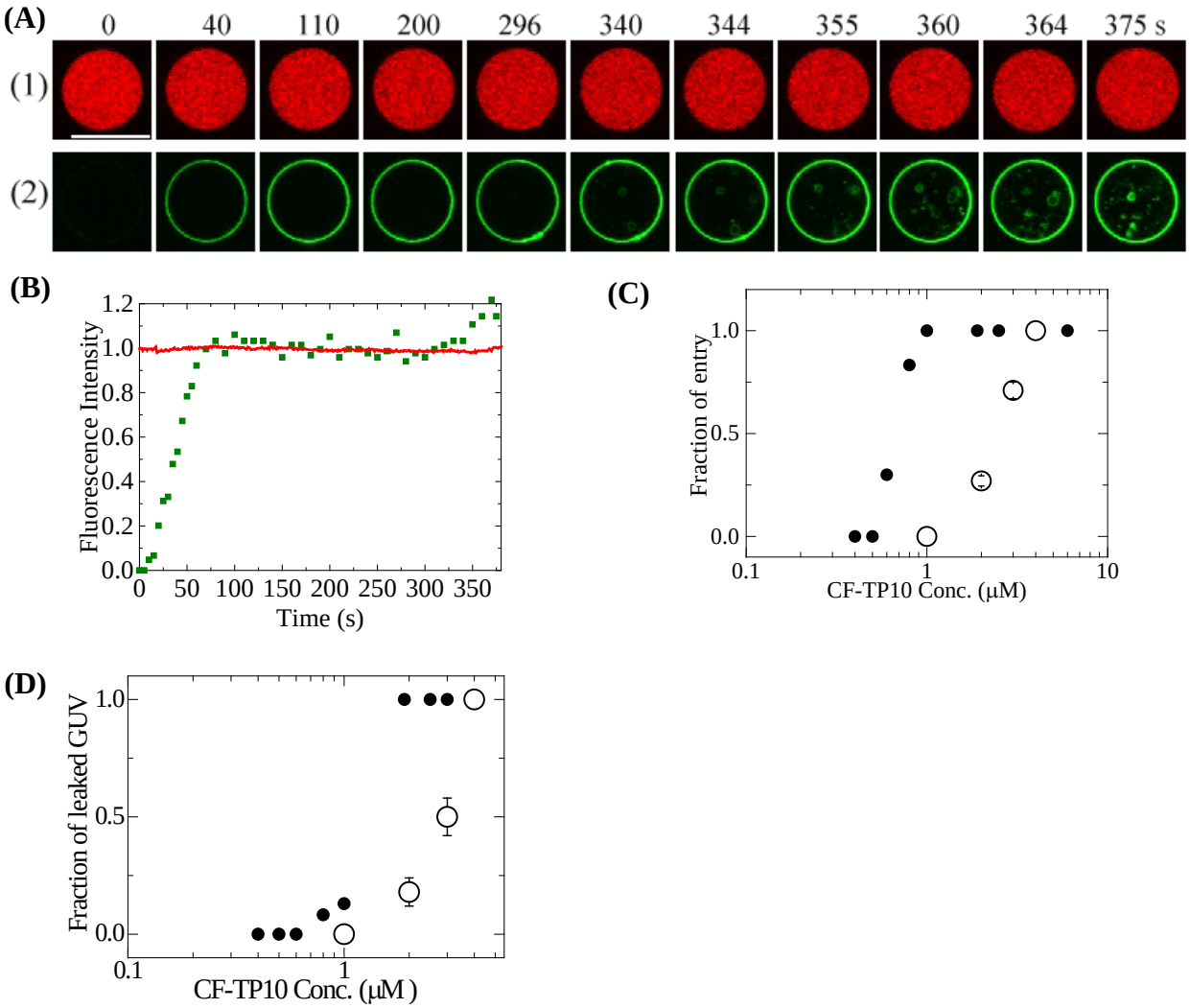

Figure-3.1: Membrane permeation of AF647 and entry of CF-TP10 into single DOPG/DOPC/chol/biotin-lipid-GUVs (20/59/40/1) containing smaller vesicles induced by CF-TP10. (A) CLSM images of (1) AF647 and (2) CF-TP10. The numbers above each image show the time in seconds after 2.0 μM CF-TP10 addition was started. The bar corresponds to 20 μm. (B) Time course of the change in normalized fluorescence intensity of the GUV shown in (A). Red and green points correspond to the fluorescence intensity of AF647 inside the GUV and of CF-TP10 in the rim of the GUV, respectively. (C) Dependence of the fraction of entry of CF-TP10 before pore formation on the concentration of CF-TP10 (○). For comparison, the data of the same dependence for 20%DOPG/79%DOPC/1%biotin-lipid-GUVs (●) are shown. (D) The dependence of the fraction of leaked GUV and the fraction of burst GUV after 6 min interaction of CF-TP10 with single GUVs on the concentration of CF-TP10 (○). The average values and standard errors of these fractions were obtained from 2 independent experiments. For comparison, the dependence of the fraction of leaked GUV for 20%DOPG/79%DOPC/ 1%biotin-lipid-GUVs (●) after 6 min interaction on the concentration of CF-TP10 are shown.

μM (○ in Figure 3.1C). The fraction of entry of CF-TP10 in these GUVs was smaller than that in the GUVs without cholesterol for the same concentration of CF-TP10 (●in Figure 3.1C) (Chapter 2). For example, 1.0 μM CF-TP10 the fraction of entry of CF-TP10 was 1.0 for GUV without cholesterol but 0.0 for the GUVs with cholesterol.

The cross-sectional area of DOPC under no tension, A_0, is 0.73 nm^2 (Nagle and Tristram-Nage, 2000) and we assume that A_0 of DOPG is same as A_0 of DOPC. A_0 of cholesterol in DOPC membranes was estimated to 0.35-0.40 nm^2 (Alwarawrah et al., 2010). Thereby A_0 of cholesterol is almost the half of A_0 of DOPC or DOPG. Based on these values, we can conclude that the surface charge density of DOPC/DOPG/chol/biotin-lipid (20/59/40/1, molar ration) is almost the same as that of 20%DOPG/80%DOPC. The cholesterol concentration in the membrane is 33 mol%, which is relatively high cholesterol concentration among various biomembrane. The results shown in Figure 3.1C clearly indicates that the presence of high concentration of cholesterol in the membrane did not inhibit the entry of CF-TP10 into a GUV but decrease the rate of entry of CF-TP10 into a GUV.

The effect of cholesterol on the CF-TP10-induced pore formation was also investigated using the leakage of AF647 shown in Figure 3.1A(1). Figure 3.1 (D) shows the fraction of leaked GUV among all the examined GUV (n = 12 to15) after the interaction of CF-TP10 with single GUV for 6.0 min (○ in Figure 3.1D). For 2.0 and 3.0 μM CF-TP10 in some GUVs rapid leakage due to rupture of GUV occurred, which are included in fraction of leaked GUV. As described in chapter 2, the fraction of leaked GUV is one of measures of evaluation of pore formation. At 1.0 μM CF-TP10, the fraction of leaked was zero and the fraction of leaked GUV increased with an increase in CF-TP10 concentration and became 1.0 at and above 4.0 μM CF-TP10 concentration. For comparison, the dependence of the fraction of leaked GUV at 6 min interaction of CF-TP10 with GUV without cholesterol is shown (●in Figure 3.1D) (Chapter 2). The results in Figure 3.1D indicate that the fraction of leaked GUV in these GUV was smaller than that in the GUVs

without cholesterol for the same concentrations of CF-TP10.

As described in chapter 2, the ability of CF-TP10 to induce pore formation is much larger than that of TP10. In this chapter, we also investigated the interaction of TP10 with single 20%DOPG/59%DOPC/40%chol/1%biotin-lipid containing water-soluble fluorescent probe, calcein using phase contrast fluorescence microscopy. Figure 3.2 A shows the effect of the interaction of 3.0 μM TP10 with single 20%DOPG/59%DOPC/40%chol/1%biotin-lipid-GUVs containing 1.0 mM calcein. Prior to TP10 addition, a phase contrast microscope image of the GUV showed high contrast (Figure 3.2A-1 and 3) due to the difference in the concentration of sucrose and glucose between the inside (0.1 M sucrose) and the outside (0.1 M glucose) of the GUV. A fluorescence microscope image of the same GUV (Figure 3.2A-2) showed a high concentration of calcein inside the GUV at this time. During addition of a 3.0 μM solution of TP10, the fluorescence intensity inside the GUV remained similar over the 360 s (Figure 3.2A-2, 3.2B). The same experiments were carried out using other single GUVs (Figure 3.2C). The data indicate that 3.0 μM solution of TP10 did not make pore in GUV membranes up to 6 min. Therefore, in the case of TP10, a fraction of leaked GUVs was 0 at and less than 3.0 μM TP10, and 0.2 at 4.0 μM TP10. These results clearly indicate that the ability of CF-TP10 to induce pore formation is much larger than that of TP10.

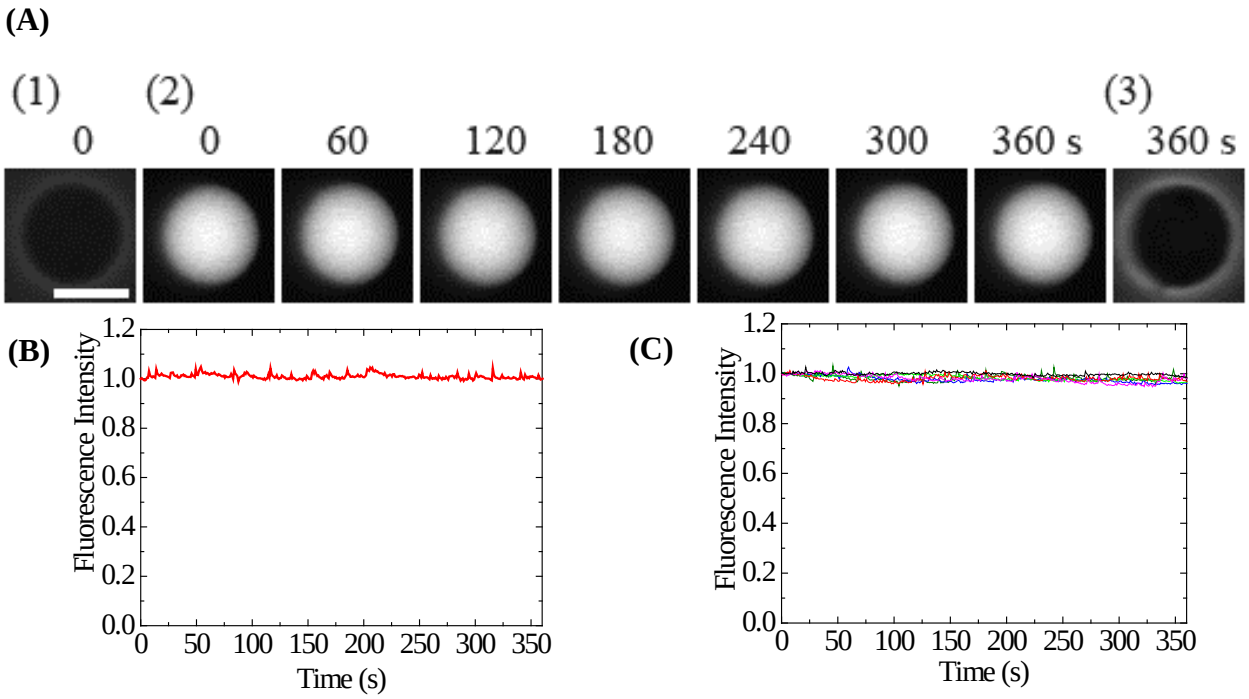

Figure-3.2: Interaction of 3.0 μM TP10 with single DOPG/DOPC/chol/biotin-lipid-GUVs (20/59/40/1). (A) Fluorescence images (2) show that the calcein concentration inside the GUV after the addition of TP10. The numbers above each image show the time in seconds after TP10 addition was started. Also shown are phase contrast images of the GUV at time 0 (1) and 360 s (3). The bar corresponds to 20 μm. (B) Time course of the normalized fluorescence intensity of the GUV shown in (A). (C) Other examples of the fluorescence intensity of calcein inside a single GUVs over time, using the same conditions as in (A).

3.3.2 Effects of cholesterol on time course of rim intensity of a GUV interacting with CF-TP10:

To elucidate the mechanism of the decrease in the rate of entry of CF-TP10 into a GUV of the membranes containing cholesterol, we investigated the interaction of CF-TP10 with GUV membranes in more details. In chapter 2, we succeeded in obtaining the rate constants of binding of CF-TP10 to a GUV membrane and of the detachment of CF-TP10 from the GUV membrane by the analysis of the time course of the rim intensity of a GUV interacting with CF-TP10. Thereby we applied this method to the present experiments. We first investigated the interaction of CF-TP10 with single 20%DOPG/59%DOPC/40%chol/1%biotin-lipid-GUVs containing AF647 using CLSM. These GUVs did not contain smaller vesicles inside the GUV, because the existence of smaller vesicles inside the GUV prevents an accurate analysis of the fluorescence intensity of the GUV rim (Chapter 2). Figure 3.3A shows a typical result of the effect of the interaction of 2.0 μM CF-TP10 with single GUVs. The CF-TP10 solution was continuously provided to the GUV surroundings through a micropipette. A fluorescence microscopic image of the GUV (Figure 3.3A (1)) shows high concentration of AF647 inside the GUV. During the addition of the 2.0 μM solution of CF-TP10, the fluorescence intensity inside GUV remained essentially constant, indicating that no pore formation occurred (red line in Figure 3.3B). On the other hand, a fluorescence microscopic image of the GUV due to the fluorescence of CF-TP10 (Figure 3.3A (2)) shows that the fluorescence intensity of the rim of the GUV (the GUV membrane) gradually increased, and that by about 100 s it is essentially saturated (green squares in Figure 3.3B).

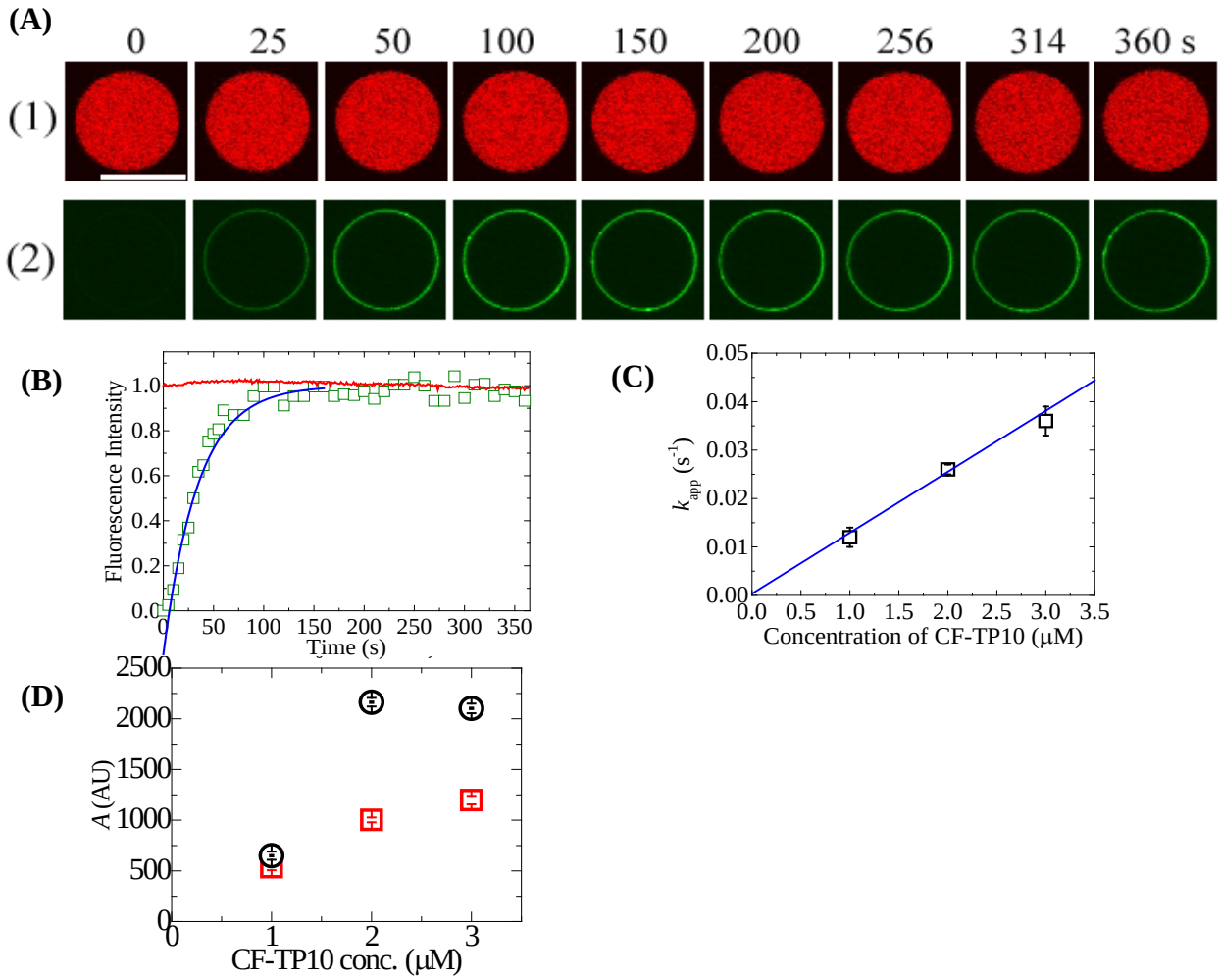

Figure-3.3: Membrane permeation of AF647 and entry of CF-TP10 into single DOPG/DOPC/chol/biotin-lipid-GUVs (20/59/40/1). (A) CLSM images of (1) AF647 and (2) CF-TP10. The numbers above each image show the time in seconds after 2.0 μM CF-TP10 addition was started. The bar corresponds to 20 μM. (B) Time course of the change in normalized fluorescence intensity of the GUV shown in (A). Red line and green squares correspond to the fluorescence intensity of AF647 inside GUV and CF-TP10 in the rim of the GUV, respectively. The solid blue line represents the best fit curve using eq. 3.1. The obtained value of k_{app} of 0.030 s^{-1}. (C) Dependence of k_{app} on CF-TP10 concentration. The time course of the charge in the fluorescence intensity of 10-15 GUVs with a diameter of 23 - 35 μm was measured. The average values and standard error of k_{app} were obtained. The solid blue line represent the best fit curve using eq. 3.2. (D) Dependence of the steady, maximum fluorescence intensity in the rim of the GUV on CF-TP10 concentration (□). They were obtained by the analysis of time course of CF-TP10 concentration in the GUV membrane such as Figure 3.3B. The average value and standard error of these fractions were obtained from two independent experiments. For comparison, the dependence of the steady, maximum fluorescence intensity in the rim of the GUV on CF-TP10 concentration for 20%DOPG/79%DOPC/1%biotin-lipid-GUVs in shown (○).

As described in chapter 2, the time course of CF-TP10 concentration in the GUV membrane, $C_M(t)$ [M] can be expressed as a following equation,

$$C_M(t) = \frac{C_M^{max}}{1+\frac{2}{K_B C_{out}^{eq}}}\left[1-\exp\{-\left(\frac{1}{2}k_{ON}C_{out}^{eq}+k_{OFF}\right)t\}\right] \quad (3.1)$$

$$= A\,[1-\exp(-k_{app}t)]$$

$$\text{where} \quad k_{app} = k_{ON}C_{out}^{eq}/2 + k_{OFF} \quad (3.2)$$

where C_{out}^{eq} is the CF-TP10 concentration in the aqueous solution outside the GUV, k_{ON} is the rate constant of the binding of CF-TP10 to a GUV membrane, k_{OFF} is the rate constant of the unbinding of CF-TP10 from the GUV membrane to the aqueous solution $K_B = k_{ON}/k_{OFF}$ is the binding constant of CF-TP10 to the lipid membrane, and k_{app} is the apparent rate constant of the increase in CF-TP10 concentration in the GUV membrane, $C_M(t)$. The time course of the fluorescence intensity of the rim of the GUV (Figure 3.3B) was fit well by eq. 3.1 (the blue line in Figure 3.3B), which gave a value for the rate constant k_{app} of 3.0 x 10^{-2} s^{-1}. We also obtained the dependence of k_{app} on CF-TP10 concentration. As expected from eq. 3.2, k_{app} increased linearly with an increase in CF-TP10 concentration, C_{out}^{eq}. Fitting the date to eq. 3.2 in figure 3.3C provided values for k_{ON} and k_{OFF}: k_{ON} = (2.5 $\pm$ 0.3) × 10^4 $M^{-1}s^{-1}$ and k_{OFF} = (0.4 $\pm$ 3.0) × 10^{-3} s^{-1} (i.e. K_B = 6.3 × 10^7 M^{-1}). Within experimental errors, both k_{ON} and k_{OFF} values for the membrane contains cholesterol were the same as those for the membrane without cholesterol [for 20%DOPG/79%DOPC/1%biotin-lipid, k_{ON} = (2.2$\pm$0.36) × 10^4 $M^{-1}s^{-1}$ and k_{OFF} = (4.0$\pm$4.0) × 10^{-3} s^{-1} (i.e. K_B = 5.2 × 10^6 M^{-1}) (Chapter 2)].

As described in chapter 2, the CF-TP10 concentration in the aqueous solution inside the GUV, C_{in}, at the initial phase can be expresses as follows.

$$V_{in} = \frac{dC_{in}}{dt} = k_{OFF}\theta_{IM}C_M^{max} \quad (3.3)$$

where V_{in} is the rate of entry of CF-TP10 into a GUV, θ_{IM} is the fraction of binding sites occupied by CF-TP10 in the monolayer, and C_M^{max} [M] is the maximum concentration of the binding site of CF-TP10 at the membrane interface of the monolayer. According to eq. 3.2, we can approximate A (i.e. the maximum value of C_M) as C_M^{max} under the conditions considered here. Figure 3.3D indicated that the value of A for 20%DOPG/59%DOPC/40%chol/1%biotin-lipid-GUVs (□ in Figure 3.3D) for various concentrations of CF-TP10, were smaller than A for 20%DOPG/79%DOPC/1%biotin-lipid-GUVs (o in Figure 3.3D). As indicated by eq. 3.3, V_{in} is proportional to C_M^{max}, and thereby we can consider that the smaller value of C_M^{max} is one of the main causes of the decrease in the rate of entry of CF-TP10 into a GUV for the membrane containing cholesterol.

3.4 CONCLUSION:

The experimental results in this chapter clearly indicate that the CF-TP10 entered the GUVs of the lipid membranes containing high concentration of cholesterol. However, the presence of high concentration of cholesterol in the membrane suppressed a little the activity of CF-TP10 to enter the GUV. The analysis of CF-TP10 surface concentration revealed that the C_M^{max} value for the membranes containing cholesterol was smaller than that of the membranes without cholesterol, which may be one of the main causes for the suppression in the activity. Plasma membranes of eukaryote contains high concentration of cholesterol, and hence the result of this chapter suggest that TP10 can translocate across the plasma membrane of eukaryote cells directly.

Chapter-4

Effects of stretching of lipid membranes on entry of transportan 10 into a single vesicle and its pore formation.

4.1 INTRODUCTION:

External forces on cells or liposomes induce lateral tension in plasma membranes or lipid membranes, which stretches them. When this tension reaches a critical value, pore formation occurs in plasma membranes of cells or lipid membranes, which induces cell death or bust of GUVs. The effect of tension due to the external forces on lipid membranes and tension-induced pore formation in lipid membranes have been investigated using GUVs (Sandre et al., 1999; Karatekin et al., 2003; Evans et al., 2003, 2011; Levadny et al., 2013; Karal et al 2015b). The binding of peptides to lipid membrane can induce tension to stretch membranes. Karal et al. reported that binding of magainin 2 to a GUV membrane induced stretching of the membrane and the rate constant of magainin 2-induced pore formation on the GUV membrane increased with an increase in stretching (Karal et al., 2015a).

In this chapter, to elucidate the mechanism of the entry of TP10 into a single GUV and its pore formation, we investigated the effects of stretching of lipid membranes on these events. To induce the stretching of lipid membranes, we applied various tensions to a GUV membranes by aspirating the GUV into a micropipette. First, we investigated the effects of binding of TP10 to a GUV membrane on its area. We found that the area of a GUV increased gradually with time when the GUV interacts with TP10 molecules and then pore formation occurred stochastically in the GUV membrane. We analysed it statistically to obtain the rate constant of TP10-induced pore formation, k_P. Next we investigated the effect of tension on the value of k_P and the area change at the pore formation. We also investigated the effect of tension on the entry of TP10 into a GUV

before pore formation. Based on these results, we discuss the effect of stretching on the TP10-induced pore formation and the entry of TP10 into a vesicle.

4.2 MATERIALS AND METHODS:

4.2.1 Chemicals:

DOPG and DOPC were purchased from Avanti Polar Lipids Inc. (Alabaster, AL). Alexa Fluor 647 hydrazide (AF647), 5-(and 6)-carboxyfluorescein (CF) succinimidyl ester, and N-((6-(biotinoyl)amino)-hexanoyl)-1,2-dihexadecanoyl-*sn*-glycero-3-phosphoethanolamine, triethyl ammonium salt (biotin-X-DHPE, referred to as biotin-lipid) were purchased from Invitrogen Inc. (Carlsbad, CA). Bovine serum albumin was purchased from Wako Pure Chemical Industry Ltd. (Osaka, Japan). TP10 and CF-labeled TP10 (i.e., CF-TP10) were synthesized and purified as described in chapter 2.

4.2.2 GUV preparation:

We prepared 20%DOPG/80%DOPC-GUVs and purified them using same method described in section 2.2.

4.2.3. Effect of the tension of lipid membranes on TP10-induced pore formation:

First, a single GUV was held at the tip of a micropipette at a constant tension in the GUV membrane for a few minutes. Then TP10 solution was continuously added from another micropipette into the vicinity of the GUV (Figure 4.1). The distance between the GUV and the tip of the micropipette was ~40 μm. We observed the GUV until it was completely aspirated into the micropipette as a result of pore formation. The time of pore formation was defined as the time when the GUV was completely aspirated; the time resolution was less than 1 s. The tension of the GUV membrane, σ, can be described as a function of ΔP, the difference in pressure

between the outside and the inside of a micropipette, as follows (Rawictz et al., 2000; Levadny et al., 2013):

$$\sigma = \frac{\Delta P d_P}{4(1 - d_P / D_V)} \tag{4.1}$$

where d_p is the internal diameter of the micropipette, and D_v is the diameter of the spherical part of the GUV exterior to the micropipette. During the addition of TP10 solution, the area of the GUV membrane increased. The fractional change in the area of the GUV membrane, δ, is $\delta = \Delta A/A_0$, where A_0 is the area of a GUV before the interaction with TP10 and ΔA is the change in the area of the GUV after the interaction with TP10. Several parameters are required to obtain δ. One parameter is the change in the projection length, $\Delta L = L_{eq} - L_0$, where L_{eq} and L_0 are steady values of projection length of the GUV during the interaction of TP10 and of the projection length before the interaction with TP10, respectively. The equation for δ is given by:

$$\delta = \frac{\Delta A}{A_0} = \frac{\Delta L d_p + D_v^2 - D_{v0}^2}{D_{v0}^2} \tag{4.2}$$

where D_V and D_{V0} are the diameter of the of the spherical part of the GUV exterior to the micropipette at equilibrium after and before the interaction with TP10, respectively.

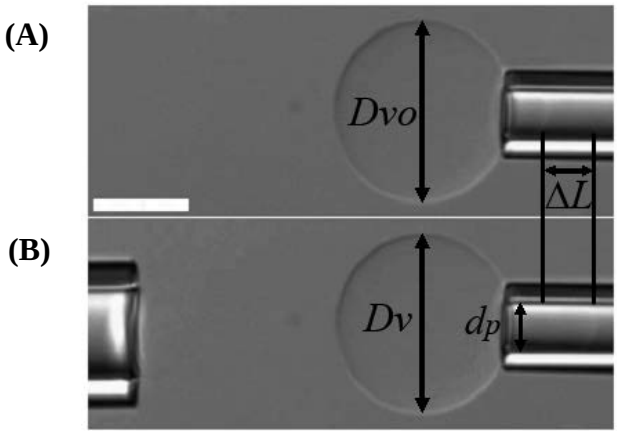

Figure-4.1: A single GUV was held at the tip of a micropipette and TP10 added from another micropipette. DIC image of a GUV fixed at the tip of a micropipette using a small aspiration pressure shown in (A). TP10 solution was continuously added from another micropipette into the vicinity of the GUV shown in (B). The bar corresponds to 20 μm.

4.2.4. Simultaneous measurement of the time course of TP10-induced change in the area of the membrane, TP10 concentration in the membrane, and membrane permeation of AF647:

The GUVs were observed using a CLSM at 25 ± 1 °C with a stage thermocontrol system. A single 20%DOPG/80%DOPC-GUV containing AF647 was held at the tip of a micropipette using a small aspiration pressure (the tension of the membrane was 0.5 mN/m), then CF-TP10 solution was continuously added from another micropipette into the vicinity of the GUV. The distance between the GUV and the tip of the micropipette was ~40 μm. The fractional change in the area of the GUV membrane, $\delta = \Delta A/A_0$, was obtained using eq. (4.2). The fluorescence intensity of the rim of the GUV was measured. First we selected only the entire rim of the GUV by two circular lines using Olympus FV10-ASW software and analyzed it. The average value of the rim intensity due to the binding of CF-TP10 in GUV membrane were obtained using this analysis.

4.3 RESULTS:

4.3.1 Effect of the tension of the lipid membrane on TP10-induced pore formation:

To reveal the role of tension in TP10-induced pore formation, we investigated the effect of tension caused by aspiration of a GUV. A single 20%DOPG/80%DOPC-GUV was held at the tip of a micropipette at a constant tension σ of 2.0 mN/m in the GUV membrane for a few minutes. Then a 1.0 μM TP10 solution was started to add. Note that 1.0 μM TP10 cannot induce a pore in a 20%DOPG/80%DOPC-GUV in the absence of tension and that a tension of 2.0 mN/m cannot induce a pore in a 20%DOPG/80%DOPC-GUV in the absence of TP10. The fractional change in area of the GUV membrane, δ , increased with time (Figure 4.2A). At 105 s the GUV was suddenly aspirated into the micropipete due to pore formation in the GUV membrane. When the same experiments were repeated using 20 single GUVs, we found that in

all the GUVs δ increased with time but pore formation occurred stochastically (Figure 4.2B). The time-course of the fraction of intact GUVs without aspiration (i.e., without pore formation) among all the examined GUVs, $P_{\text{intact}}(t)$, could be fit well by a single exponential decay function as follows (Figure 4.2C):

$$P_{\text{intact}}(t) = \exp\left(-k_{\text{p}}(t - t_{\text{eq}})\right) \qquad (4.3)$$

where k_{p} is the rate constant of TP10-induced pore formation in the presence of constant tension caused by aspiration of a GUV and t is the time that TP10 solution started to add to the vicinity of the GUV, and t_{eq} is an adjustable parameter which depends on the binding time of TP10 with the GUV membrane. From this fitting, the value of k_{p} was determined to be $1.8 \times 10^{-2}\,\text{s}^{-1}$ and $0.4 \times 10^{-2}\,\text{s}^{-1}$ for 1.0 μM TP10 at σ = 2.0 and 0.5 mN/m, respectively. Using the same method we investigated the effects of various tensions on the TP10-induced pore formation. For 1.0 μM TP10, k_{p} increased with tension (Δ) σ = 0.5 mN/m and (□) σ = 2.0 mN/m in Figure 4.2 C). We also investigated the effects of tension on pore formation induced by different concentrations of TP10. At the same concentration of TP10, k_{p} increased with tension (Figure 4.2D), and at same tension k_{p} increased with TP10 concentration (Figure 4.2 E). These results indicate that stretching of the lipid membranes (or tension in the membranes) due to an external force elevates the k_{p} value. We investigated the time course of fractional area change in 20%DOPG/80%DOPC -GUVs at σ = 2.0 mN/m with various concentrations of TP10 (1.0, 0.5, 0.1 μM) (Figure 4.2 F). The results clearly show that pore formation occurred within 100 s for 1.0 μM TP10, but for lower concentration of TP10 (0.1 μM), it occurred after 300s. The slope of curves (i.e., the rate of the increase in δ in Figure 4.2 F) increased with an increase in TP10 concentration. Moreover, the average fractional area change of the GUV membrane at the time when pore formation occurred in the GUV membrane, δ_1^*, increased with an increase in TP10 concentrations at the same tension (Figure 4.2 G). In contrast, at the same TP10 concentration δ_1^* decreased with an increase in tension (Figure 4.2 H).

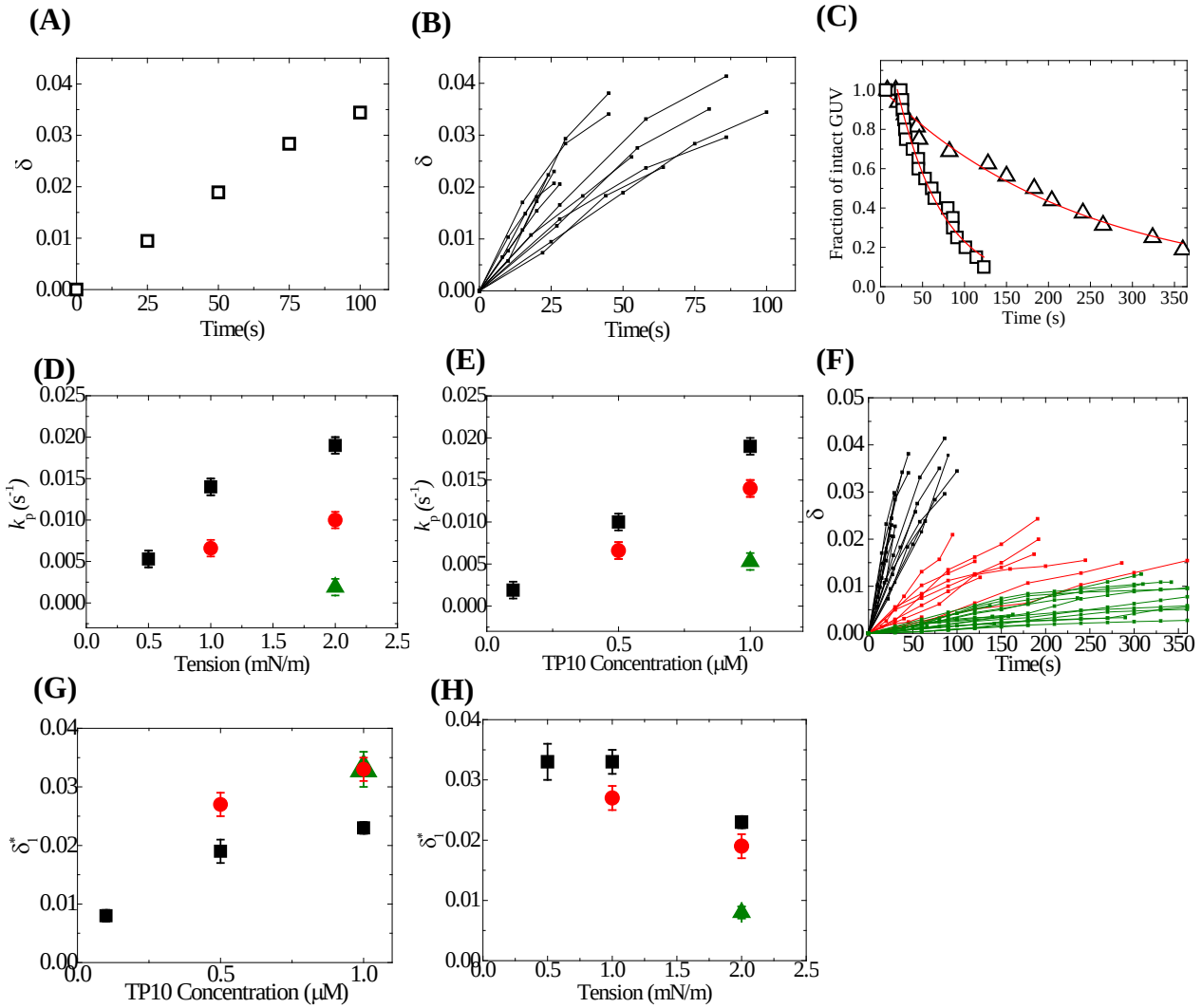

Figure-4.2: The effect of tension caused by an external force on TP10-induced pore formation in single 20%DOPG/80%DOPC-GUVs. (A) Time course of fractional area change in GUVs at σ = 2.0 mN/m during the addition of 1.0 μM TP10. (B) Other examples of time course of fractional area change in GUVs under the same conditions of (A). Each curve corresponds to the data of each GUV. (C) Time course of the fraction of intact GUVs during addition of 1.0 μM TP10 among all the examined GUVs, $P_{intact}(t)$, at σ = 0.5 mN/m (Δ), 2.0 mN/m (□). Twenty single GUVs were examined in each experiment. The red solid line represents the best fit curve of eq. (4.3). (D) Dependence of k_p on tension with various concentrations of TP10; (■) 1.0 μM, (●) 0.5 μM, and (▲) 0.1 μM. (E) Dependence of k_p on TP10 concentration at various tension; σ = 2.0 mN/m (■), 1.0 mN/m, (●) and 0.5 mN/m (▲). The average values and standard error for k_p were determined from 2-3 independent experiments using 20 GUVs. (F) Time course of fractional area change in GUVs at σ = 2.0 mN/m during the addition of various concentrations of TP10; (■) 1.0 μM, (■) 0.5 μM, and (■) 0.1 μM. Each curve corresponds to the data of each GUV. (G) Dependence of δ_1^* on TP10 concentration at constant tension; σ = 2.0 mN/m (■), 1.0 mN/m (●), and 0.5 mN/m (▲). (H) Dependence of δ_1^* on tension at the same TP10 concentration; (■) 1.0 μM, (●) 0.5 μM, and (▲) 0.1 μM.

4.3.2 Correlation of time course of the CF-TP10 concentration in the GUV membrane and its area change in the presence of tension:

To obtain information on time course of the CF-TP10 concentration in the GUV membrane, we investigated the interaction of CF-TP10 with single 20%DOPG/80%DOPC-GUVs containing AF647 in the GUV lumen using CLSM. Figure 4.3A shows a typical result of the effect of the interaction of 0.3 μM CF-TP10 with single GUVs at σ = 1.0 mN/m. The CF-TP10 solution was continuously provided to the GUV surroundings through a micropipette. A fluorescence microscope image of the GUV (Figure 4.3A (1)) shows a high concentration of AF647 inside the GUV before the interaction. During the addition of the 0.3 μM solution of CF-TP10, the fluorescence intensity inside the GUV remained essentially constant over the first 256 s, and at 257 s the fluorescence intensity suddenly decreased because the GUV was aspirated into the micropipette (Figure 4.3A (1) & red curve in Figure 4.3B). This result indicates directly that no leakage of AF647 occurred before the aspiration of the GUV and thereby the definition of the pore formation in the previous section (i.e., the time when a GUV is aspirated into a micropipette is the time of TP10-induced pore in lipid membranes) is correct.

On the other hand, a fluorescence microscope image of the GUV due to the fluorescence of CF-TP10 (Figure 4.3A (2)) shows that the fluorescence intensity of the rim of the GUV (the GUV membrane) gradually increased, and at about 225 s it was almost saturated (green lines in Figure 4.3B). Since the fluorescence intensity of the rim of the GUV is proportional to CF-TP10 concentration in the GUV membrane, C_M, this result indicates that C_M increased gradually with time and was almost saturated. The time course of δ was also measured simultaneously (□ in Figure 4.3B). The values of δ increased with time, but the rate of the increase in δ was slower than that of C_M. When the same experiment was repeated with other CF-TP10 concentrations (0.5 and 0.7 μM), C_M increased with time more rapidly at higher CF-TP10 concentration. That is, the rate of increase in C_M was larger at higher CF-TP10 concentration.

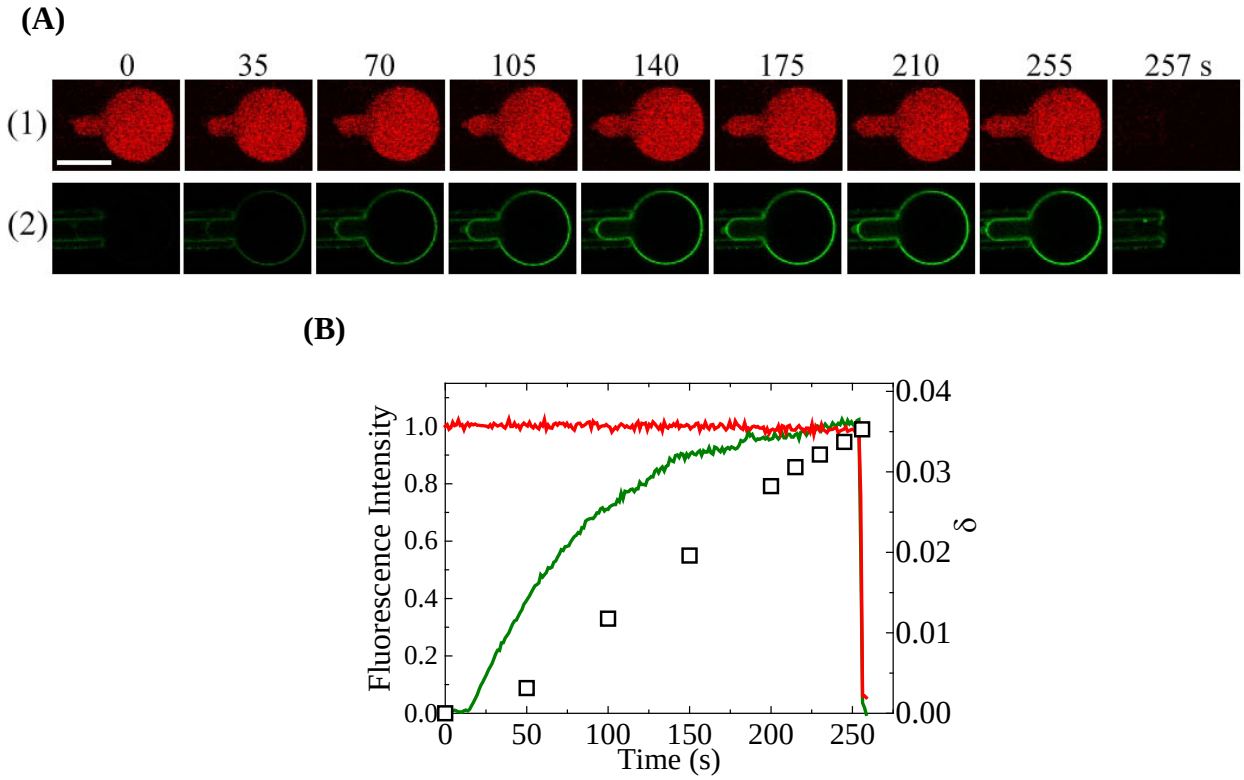

Figure-4.3: Leakage of AF647 and CF-TP10 concentration of the membrane in single 20%DOPG/80%DOPC-GUVs interacting with CF-TP10 in the presence of tension. (A) CLSM images of (1) AF647 and (2) CF-TP10 of a GUV during the interaction of 0.3 μM CF-TP10 at σ = 1.0 mN/m. The numbers above each image show the time in seconds after CF-TP10 addition was started. The bar corresponds to 30 μm. (B) Time course of the change in normalized fluorescence intensity of the GUV shown in (A). Red, green line and □ correspond to the fluorescence intensity of AF647 inside the GUV, CF-TP10 in the rim of the GUV, and fractional area change of GUV, respectively.

4.3.3 Effect of the tension on entry of CF-TP10 into single GUV:

To reveal the effect of tension on entry of TP10 into a single GUV, we applied the method developed in chapter 2. To elucidate whether CF-TP10 enter the inside of a GUV, we monitored the fluorescence intensity of smaller vesicles inside the GUV using CLSM. First a single 20%DOPG/80%DOPC-GUV containing smaller vesicles of the same membrane and containing AF647 was held at the tip of a micropipette at a specific constant tension in the GUV membrane for a few minutes. Then a specific concentration of CF-TP10 solution was started to add to the vicinity of the GUV. Figure 4.4A shows a typical experimental result of the effect of the tension of 1.0 mN/m on the interaction of 0.60 μM CF-TP10 with a single GUV. Before the aspiration of a GUV into a micropipette, the fluorescence intensity of the inside of the GUV due to AF647 kept constant, indicating that the membrane permeation of AF647 did not occur (Figure 4.4A(1), B). On the other hand, Figure 4.4A(2) shows that the fluorescence intensity of the GUV membrane gradually increased. At the beginning of the interaction, there was no fluorescence inside the GUV, but after 133 s, fluorescence intensity was observed due to the membranes of the smaller vesicles inside the GUV (t = 133, 153, 160 s in Figure 4.4A(2)). This fluorescence occurred before CF-TP10-induced pore formation (166 s). These results indicate that CF-TP10 entered the inside of the GUV from the outside by translocating across the GUV membrane and then bound to the membrane of the smaller vesicles inside the GUV, as discussed in Chapter 2. The entry of CF-TP10 into the inside of the GUV occurred before pore formation at 6 min. To evaluate the activity of entry of CF-TP10 into a GUV, we can use the fraction of entry of CF-TP10, which is the fraction of the GUVs where entry of CF-TP10 is observed before pore formation (see chapter 2). When the same experiments were repeated using 10-15 single GUVs, we observed almost the same results as Figure 4.4A and 4.4B, and found that the fraction of entry of CF-TP10 at 6 min of the interaction of CF-TP10 with the GUV was 0.38. In contrast, in the absence of tension 0.6 μM CF-TP10 did not enter into a 20%DOPG/80%DOPC-GUV within

6 min interaction. We also investigated the effect of tension on the entry of CF-TP10 into a GUV during the interaction of other concentrations of CF-TP10 (Figure 4.4C). At and above 0.3 μM CF-TP10, the entry of CF-TP10 was observed in some examined GUVs in the presence of tension, and the fraction of entry of CF-TP10 increased with an increase in tension and became 0.6 at 0.75 mN/m for 0.6 μM CF-TP10. However, the fraction of entry decreased at higher tension (σ = 1.0 mN/m) and 0.6 μM CF-TP10 concentration. It may be explained by the rapid pore formation at the higher tension.

When we made the same experiments using 20%DOPG//79%DOPC/ 1%biotin-lipid-GUVs, the results were similar to the 20%DOPG//80%DOPC-GUVs (Figure 4.4C).

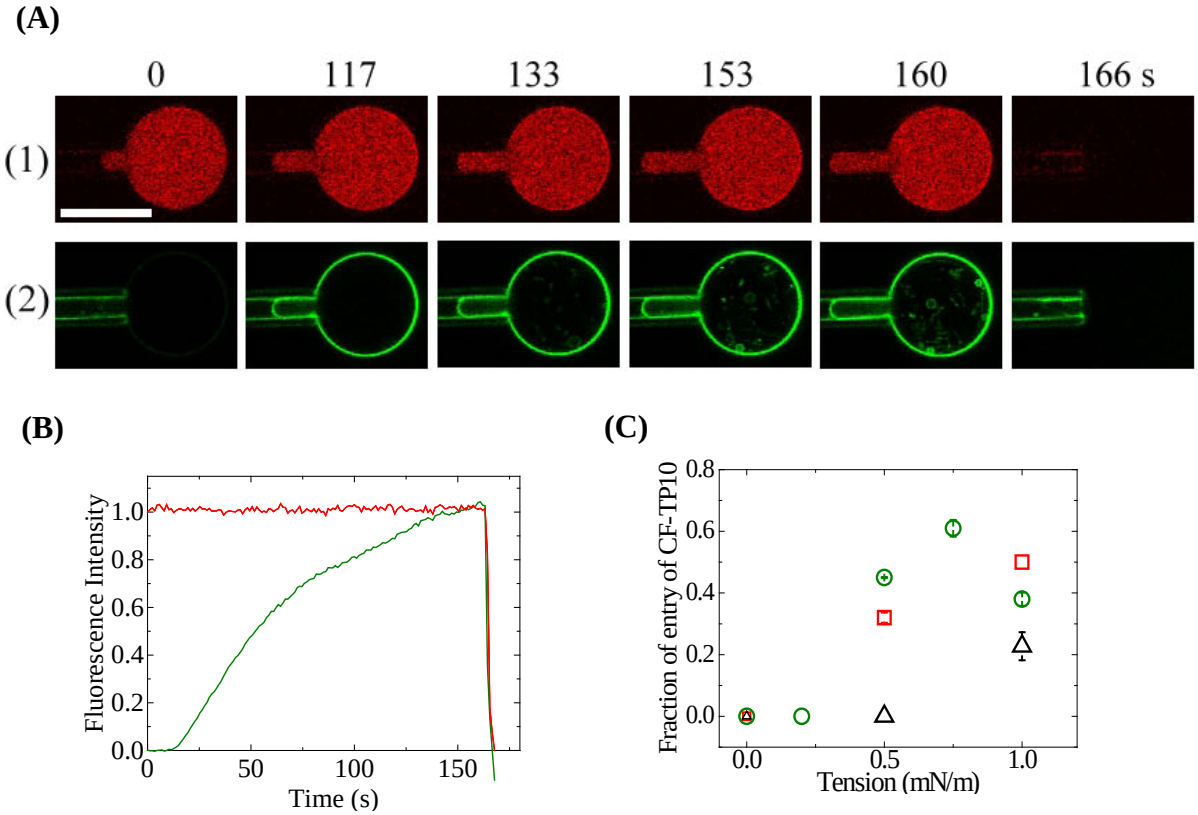

Figure 4.4: The effect of tension caused by an external force on entry of CF-TP10 into single 20%DOPG/80%DOPC-GUVs. (A) Time course of fluorescence intensity due to AF647 and CF-TP10 in 20%DOPG/80%DOPC-GUVs at σ = 1.0 mN/m during the addition of 0.6 μM CF-TP10. CLSM images of (1) AF647 and (2) CF-TP10. The numbers above each image show the time in seconds after CF-TP10 addition was started. The bar corresponds to 30 μm. (B) Time course of the change in normalized fluorescence intensity of the GUV shown in (A). Red and green line correspond to the fluorescence intensity of AF647 inside the GUV and of CF-TP10 in the rim of the GUV, respectively. (C) Dependence of fraction of entry of CF-TP10 at 6 min on tension. (o) 0.6 μM, (□) 0.5 μM, and (Δ) 0.3 μM CF-TP10 concentrations. The average values and standard error for fraction of entry of CF-TP10 at each tension were determined from two independent experiments using 10-15 GUVs.

4.4 DISCUSSION:

The results in this chapter clearly indicate that the binding of TP10 increased the area of the membrane and pore formation occurred stochastically when the fractional area change of the GUV membrane, δ, reached near a critical value (Figure 4.2F). As described in chapter 2, TP10 molecules enter into a single GUV before TP10-induced pore formation. These results suggest that TP10 molecules bind with the interface of both the monolayers of the GUV, i.e., the outer and the inner monolayers, before pore formation, which may contributes the increase in δ. At constant tension, δ_1^* increased with an increase of TP10 concentration (Figure 4.2 G) and k_P increased with an increase in TP10 concentrations (Figure 4.2 E). Therefore k_P increased with an increase in δ_1^* at constant tension. On the other hand, at constant TP10 concentration, δ_1^* decreased with tension (Figure 4.2 H), and k_P increased with tension (Figure 4.2 D). Therefore, k_P increased with a decrease in δ_1^* at constant TP10 concentration. To understand this apparently contradict phenomena, we consider the effect of tension next.

Tension due to the external force induces the stretching of lipid membranes. Hence, we have to consider two factors to induce an increase in fractional area change, δ, when TP10 interacts with GUVs in the presence of tension due to the external force. One is the fractional area change due to the interaction of TP10 with the membrane, δ_1, and the other is the fractional area change due to the tension causing external force, δ_2. It is well known that $\delta_2 = \sigma/K_a$, where K_a is the elastic (compressibility) modulus of a bilayer. We obtained the elastic modulus of the 20%DOPG/80%DOPC membrane under the same conditions using the standard method (K_A = 141 $\pm$ 10 mN/m). Using this value, we obtained the δ_2 value corresponding to various σ values. If we assume that the effects of two factors are independent, we can obtain the critical values of total fractional area change of the GUV membrane at which pore formation occurred in the GUV membranes, δ_t^*, using $\delta_t^* = \delta_1^* + \delta_2$. Table 4.1 summaries the value of δ_1^*, δ_2 and δ_t^*. At the same TP10 concentration, the δt^* values were the same irrespective of tension (Figure 4.5A),

because δ_1* decreased with an increase in tension at the same TP10 concentration (Table 4.1). If we consider the results of Figure 4.2 D and 4.5 A together, we can conclude that k_P increased with an increase in tension at same TP10 concentrations. With an increase in tension, the time required for further increase in δ decreased because the initial area change due to the tension increased with tension, and hence k_P increased.

At the same tension, δ_t* increased with an increase in TP10 concentration (Figure 4.5 B). For example, at σ = 2.0 mN/m, δ_t* are 0.022 $\pm$ 0.001, 0.033 $\pm$ 0.002, and 0.038 $\pm$ 0.001 for 0.10 μM, 0.50 μM, and 1.0 μM TP10, respectively. On the other hand, the experimental results show that the rate of rising δ increased with TP10 concentration (Figure 4.2F). As described above, the binding of TP10 to a GUV membrane induces stretching of the membrane and the rate of binding of TP10 with membranes increased with an increase in TP10 concentration. Therefore, the rate of rising δ increased with an increase in TP10 concentration. It is considered that pore formation in lipid membrane occurs through thermal fluctuation of lateral density of lipid membranes and thereby it takes some time for pore formation at a critical δ (Levadny et al., 2013). Therefore, if the rate of rising δ, is large, δ increases further before pore formation. This is why δ_t* increased with an increase in rising δ. Similar phenomena were observed in the tension-induced pore formation in a GUV membrane with various loading rate (i.e., the rate of the increase in tension in the membrane) using the dynamic tension spectroscopy (Evans et al., 2003). They found that the rupture tension increased with loading rate. Since δ is proportion to tension, the rate of rising δ and δ_t* in this thesis correspond to the loading rate and the rupture tension in Evans's results, respectively. Therefore, the mechanism of the effect of the rate of raising δ on δ_t* may be the same as that of the effect of the loading rate on the rupture tension.

The fraction of entry of TP10 before pore formation at 6 minutes increased with an increase in tension of the membranes induced by the aspiration of the GUV (Figure 4.4C). As described in eq. 3.3 of chapter 3, the rate of entry of CF-TP10 into a GUV, V_{in}, is proportional to

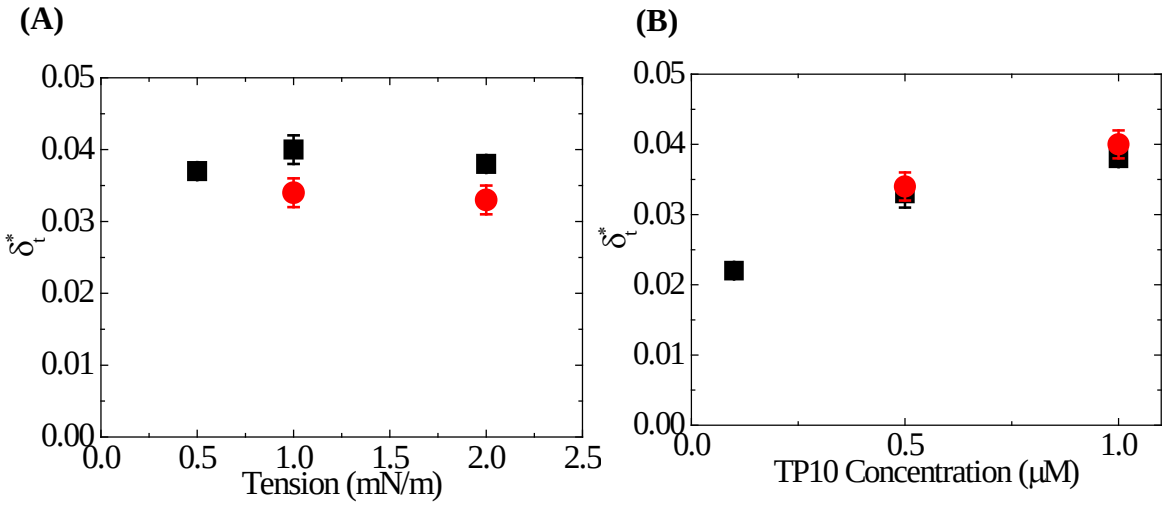

Figure-4.5: Dependence of average critical values of total fractional area change of the GUV membrane, δ_t^* on tension and TP10 concentration. (A) Dependent of δ_t^* on tension at the same TP10 concentrations; (■) 1.0 μM, and (●) 0.5 μM. The average values and standard error for δ_t^* were determined from two to four independent experiments using 12-22 GUVs. (B) Dependence of δ_t^* on concentration of TP10 at the same tension σ = 2.0 mN/m (■), and 1.0 mN/m (●).

Table-4.1: Dependence of δ_1^*, δ_2 and δ_t^* on tension and TP10 concentration:

TP10 Concentration (μM)	δ_1^*	δ_2	δ_t^*
Tension 2.0 mN/m			
1.0	0.023 ± 0.001	0.014 ± 0.001	0.038 ± 0.001
0.5	0.019 ± 0.002	0.014 ± 0.001	0.033 ± 0.002
0.1	0.008 ± 0.001	0.014 ± 0.001	0.022 ± 0.001
Tension 1.0 mN/m			
1.0	0.033 ± 0.002	0.0071 ± 0.001	0.040 ± 0.002
0.5	0.027 ± 0.002	0.0071 ± 0.001	0.034 ± 0.002
Tension 0.5 mN/m			
1.0	0.033 ± 0.003	0.0035 ± 0.0004	0.037 ± 0.003

δ_1^* is define as the fractional area change of the GUV membrane at the time when pore formation occurred in the GUV membrane, δ_2 is the fractional area change of the GUV membrane due to the applied external tension and δ_t* is the critical values of total fractional area change of the GUV membrane at which pore formation occurred in the GUV membranes.

k_{OFF} and C_M^{max}. However, at present we don't have sufficient data of k_{OFF} and C_M^{max} values. To elucidate the mechanism of the effect of stretching on the entry of CF-TP10 into a GUV, we need further studies in future.

4.5 CONCLUSION:

The results in this chapter clearly indicate that the binding of TP10 to a GUV membrane induced stretching of the membrane and during an increase in stretching pore formation occurred stochastically in the membrane. For the same TP10 concentration, the average fractional area change at a time when pore formation occurred, δ_t*, were the same irrespective of the tension due to the external force. Thereby we conclude that δ_t* is one of the important factors for the TP10-induced pore formation. With an increase in tension, the time required for further increase in area change decreased because the initial area change increased with tension, and hence the rate constant of pore formation increased. On the other hand, for the same tension, δ_t* increased with an increase in TP10 concentration. This may be explained by the increase in the rate of rising δ, which is similar to the loading rate. We also conclude that tension increased the fraction of entry of CF-TP10 into a GUV before pore formation, and hence the rate of entry of CF-TP10 into a single GUV is increased, although its mechanism is unclear at present.

Chapter-5

General Conclusion

A new method has been developed to detect the entry of TP10 into a single GUV using confocal microscopy. Using this method, it was found that the CF-TP10 molecules entered a single GUV before CF-TP10-induced pore formation. The fraction of entry of CF-TP10 increased with an increase in CF-TP10 concentration. Moreover, at a lower concentration of CF-TP10, pore formation did not occur after the translocation of CF-TP10, indicating that the entry of TP10 into a GUV and TP10-induced pore formation are not related, i.e., some other factor is necessary for pore formation. Based on the analysis of the fluorescence intensity of the GUV membrane due to CF-TP10, the rate constants of binding and unbinding of TP10 with lipid membrane were obtained. The information on the size of TP10-induced pore was also obtained. The fluorescence probe, TRD 40K, passed through the TP10-induced pore, indicating that the radius of TP10 induced pore is larger than 5.0 nm. This result supports that the TP10 can deliver larger cargo molecules such as proteins or oligonucleotides into cells or vesicles.

Plasma membranes of eukaryote contains high concentration of cholesterol and thereby it is important to know whether TP10 can enter single GUVs or not. CF-TP10 entered GUVs containing cholesterol before leakage of AF647, although higher concentrations of TP10 were required compared with GUVs without cholesterol. Therefore, TP10 has an ability to translocate across the membrane of eukaryote cells and deliver the cargo molecules into the living cells.

The binding of TP10 to a GUV membrane induced stretching of the membrane and during an increase in stretching pore formation occurred stochastically in the membrane. The fractional area change of a GUV membrane played an important role in the TP10-induced pore formation. Tension due to the external force decreased TP10-concentration required for the pore

formation, and also increased the fraction of entry of CF-TP10 into a GUV before pore formation, and hence the rate of entry of CF-TP10 into a single GUV was increased.

The above results indicate that TP10 has an ability to translocate across the lipid membrane before TP10-induced pore formation in the lipid membrane, even if high concentrations of cholesterol exist in the membranes. It is the first direct observation of translocation of TP10 through the lipid membrane and enters into lipid vesicles. The large size of the TP10-induced pore supports that TP10 can deliver the large cargo molecules into cells.

Chapter-6

References

Alam, J. M., Kobayashi, T., and Yamazaki, M. (2012) Single Giant Unilamellar Vesicle Method Reveals Lysenin-Induced Pore Formation in Lipid Membranes Containing Sphingomyelin. *Biochemistry* 51, 5160-5172.

Alwarawrah, M., Dai, J., and Huang, J. (2010), A Molecular View of the Cholesterol Condensing Effect in DOPC Lipid Bilayers, *J. Phys Chem B.* 114, 7516–7523.

Arsov, Z., Nemec, M., Schara, M., Johansson, H., Langel, U., and Zorko, M. (2008) Cholesterol prevents interaction of the cell-penetrating peptide transportan with model lipid membranes, *J. Pept. Sci.* 14, 1303–1308.

Barany-Wallje, E., Gaur, J., Lundberg, P., Langle, Ű., and Gräslund, A. (2007) Differential membrane perturbation caused by the cell penetrating peptide TP10 depending on attached cargo. *FEBS Lett.* 581, 2389-2393.

Baumgart, T., Hess, S. T., and Webb, W. W. (2003) Imaging coexisting fluid domains in biomembrane models coupling curvature and line tension. *Nature* 425, 821-824.

Bloom, M., and Mouritsen, O. G. The evolution of membranes, in: R. Lipowsky, E. Sackmann (Eds.), in *Structure and dynamics of membranes*, Elsevier Science B. V., Amsterdam, **1995**, pp. 65-95.

Boll, A., Jatho, A., Czudnochowski, N., Geyer, M., and Steinem, C. (2011) Mechanistic insights into the translocation of full length HIV-1 Tat across lipid membranes. *Biochim. Biophys. Acta.* 1808, 2685-2693.

Bárány-Wallje, E., Gaur, J., Lundberg, P., Langel, Ü, and Gräslund, A. (2007) Differential membrane perturbation caused by the cell penetrating peptide Tp10 depending on attached cargo, *FEBS Letters* 581, 2389–2393.

Delcroix, M., and Riley, L. W. (2010) Cell-Penetrating Peptides for Antiviral Drug Development, *Pharmaceuticals* 3, 448–470.

Derossi, D., Joliot, A. H.,Chasseing, G., and Prochiantz, A., (1994) The third helix of the Antennapedia homeodomain translocates through biological membranes. *J. Biol. Chem.* 269, 10444-10450.

Deryagin, B. V. and Gutop, Y. V. (1962) Theory of the breakdown (rupture) of free films. *Kolloidn. Zh.* 24, 370−374.

Dietz, G. P., and Bähr, M. (2004) Delivery of bioactive molecules in the cell: the Trojan horse approach, *Mol,.Cell. Neurosci.* 27, 85-131.

Dos Santos Cabrera, M. P., Alvares, D.S., Leite, N. B., de Souza, B.M., Palma, M.S., Riske, K. A., and Neto, J.R. (2011) New insight into the mechanism of action of wasp mastoparan peptides: lytic activity and clustering observed with giant vesicles. *Langmuir* 27, 10805-10813.

Drin, G., Cottin, E. Blanc, Rees, A. R., and Temsamani, J. (2003) Studies on the internalization mechanism of cationic cell-penetrating peptides, *J. Biol. Chem.* 278, 31192-31201.

Dunkin, C. M., Pokorny, A., Almeida, P. F., and Lee, H. S. (2011), Molecular dynamics Studies of transportan 10 (Tp10) interacting with a POPC lipid lilayer, *J. Phys Chem B.* 115, 1188–1198.

E.L.-Andaloussi, S., Johansson, H., Magnusdottir, A., Järver, P., Lundberg, P., and Langel, Ü. (2005) TP10, a delivery vector for decoy oligonucleotides targeting the Myc protein, *J. Control. Release* 110, 189– 201.

Evans E., Heinrich, V., Ludwig, F., and Rawicz, W. (2003) Dynamic tension spectroscopy and strength of biomembranes. *Biophys J.* 85, 2342-2350.

Evans, E., and Smith, B. A. (2011) Kinetics of hole nucleation in biomembrane rupture. *New J. Phys.,* 13, 095010.

Fanghänel, S., Wadhwani, P., Strandberg, E., Verdurmen, W. P. R., Bürck, J., Ehni, S., Mykhailiuk, P. K., Afonin, S., Gerthsen, D., Komarov, I. V., Brock, R. and Ulrich, A. S. (2014) Structure Analysis and Conformational Transitions of the Cell Penetrating Peptide Transportan 10 in the Membrane-Bound State, *PLOS ONE* 9, e99653.

Fischer, R., Köhler, R., Fotin-Mleczek, M., F. K., and Brock, R. (2004) A stepwise description of the intercellular fact of cationic cell-penetrating peptides, *J. Biol. Chem.* 279, 12625-12635.

Foerg, C., and Merkle, H. P. (2008) On the biomedical promise of cell penetrating peptides: Limits versus prospects, *J. Pharm. Sci.* 97, 144–162.

Milletti, F. (2012) Cell-penetrating peptides: classes, origin, and current landscape, *Drug Discov. Today* 17, 850–860.

Frankel, A. D., and Pobo, C. O. (1988) Cellular uptake of the TAT protein from human immunodeficiency virus, *Cell* 55, 1189-1193.

Fuchs, S. M. and Raines, R. T. (2004) Pathway for polyarginine entry into mammalian cell, *Biochemistry* 43, 2438-244.

Fuertes, G., Garcia-Sáez, A., Esteban-Martin, S., Giménez, D., Sánchez-Muñoz, O. L., Schwille, P., and Salgado, J. (2010) Pores formed by Baxα5 relax to a smaller size and keep at equilibrium. *Biophys. J.* 99, 2917-2925.

Gaidukov, L., Fish, A., and Mor, A. (2003) Analysis of membrane-binding properties of dermaseptin analogues: relationships between binding and cytotoxicity. *Biochemistry* 42, 12866-12874.

Green, M., and Loewenstein, and P. M., (1988), Autonomus functional domains of chemically synthesized human immunodeficiency virus Tat trans-activator protein, *Cell* 55, 1179-1188.

Janely Pae, J., Säälik, P., Liivamägi, L., Lubenets, D., Arukuusk, P., Langel, Ülo, and Pooga, M. (2014) Translocation of cell-penetrating peptides across the plasma membrane is controlled

by cholesterol and microenvironment created by membranous proteins. *J. Control Release* 192, 103–113.

Nagle, J. F. and Tristram-Nagle, S. (2000) Structure of lipid bilayers, *Biochim. Biophys. Acta*, 1469, 159-195.

Jobina, M. L., Bonnafousa, P., Temsamania, H., Doleb, F., Grélarda, A., Dufourca, E. J., and Alves, I. D. (2013) The enhanced membrane interaction and perturbation of a cell penetrating peptide in the presence of anionic lipids: Toward an understanding of its selectivity for cancer cells, *Biochim. Biophys. Acta: Biomembr.* 1828, 1457-1470.

Karatekin, E.; Sandre, O.; Guitouni, H.; Borghi, N.; Puech, P. -H.; Brochard-Wyard, F. (2003) Cascades of transient pores in giant vesicles: line tension and transport. *Biophys. J.*, 84, 1734−1749.

Karal, M. A. S.[a], Alam, J. M., Takahashi, T., Levadny, V., and Yamazaki, M. (2015) Stretch-Activated Pore of Antimicrobial Peptide Magainin 2, *Langmuir* 31, 3391-3401.

Karal, M. A. S.[b], Levadny, V., Tsuboi, T., Belaya, M., and Yamazaki, M. (2015) Electrostatic interaction effects on tension-induced pore formation in lipid membranes, *Phys. Rev. E*, 92, 012708 (7 pages).

Kobayashi, S., Takeshima, K., Park, C. B., Kim, S. C., and Matsuzaki, K. (2000) Interactions of the Novel Antimicrobial Peptide Buforin 2 with Lipid Bilayers: Proline as a Translocation Promoting Factor, *Biochemistry* 39, 8648-8654.

Langel, Ü., Pooga, M., Kairane, C., Zilmer, M., and Bartfai, T. (1996) A galanin-mastoparan chimeric peptide activates the Na+, K(+)-ATPase and reverses its inhibition by ouabain, *Regul. Pept.* 62, 47-52.

Lee, M.-T., Sun, T.-L., Hung, W.-C., and Huang, H. W. (2013) Process of inducing pores in membranes by melittin. *Proc. Natl. Acad. Sci. USA* 110, 14243-14248.

Leontiadou, H., and Mark A. E., and Marrink, S. J. (2006) Antimicrobial peptides in action. *J. Amer. Chem. Soc.* 128, 12156-12161.

Levadny, V., Tsuboi, T., Belaya, M., and Yamazaki, M. (2013) Rate Constant of Tension-Induced Pore Formation in Lipid Membranes. *Langmuir* 29, 3848-3852.

Li. W., Nicol, F., and Szoka F. C. Jr. (2004) GALA: A designed synthetic pH-responsive amphipathic peptidewith applications in drug and gene delivery. *Adv. Drug Deliv. Rev.* 56, 967–985.

Lindgren, M., Hällbrink, M., Elmquist, A. and Langel, Ü. (2004) Passage of Cell-penetrating peptides across a human epithelial cell layer in vitro, *Biochem. J.* 377, 69-76.

Lister, J. D. (1975) Stability of lipid bilayers and red blood cell membranes. *Phys. Lett.* A53, 193−194.

London E. How principles of domain formation in model membranes may explain ambiguities concerning lipid raft formation in cells. *Biochim. Biophys. Acta* 2005; 1746: 203–220.

Lopez, C. F., Nielsen, S. O., Srinivas, G., DeGrado, W. F., and Klein, M. L. (2006) Probing membrane insertion activity of antimicrobial polymers via coarse-grain molecular dynamics. *J. Chem. Theory and Comput.* 2, 649-655.

Lundberg, P., Magzoub, M., Lindberg, M., Hällbrink, M., Jarvet, J., Eriksson, L. E. G., Langel, Ü., and Gräslund, A. (2002) Cell membrane translocation of the N-terminal (1-28) part of the prion protein. *Biochem. Biophys. Res. Commun.* 299, 85-90.

Madani, F., Lindberg, S., Langel, Ü., Futaki, S., and Gräslund, A. (2011) Mechanisms of Cellular Uptake of Cell-Penetrating Peptides, *J. Biophys.* 2011, 414729.

Magzoub, M., and Gräslund, A. (2004) Cell-Penetrating Peptides: small form inception to application, *Q. Rev. Biophys.* 37, 147-195.

Maiolo, J. R., Ferrer, M., and Ottinger, E. A. (2005) Effects of cargo molecules on the cellular uptake of arginine-rich cell-penetrating peptides, *Biochim. Biophys. Acta*, 1712, 161 – 172.

Marks, J. R., Placone, J., Hristova, K., and Wimley W. C. (2011) Spontaneous membrane-translocating peptides by orthogonal high-throughput screening. *J. Am. Chem. Soc*. 133, 8995–9004.

Mishraa, A., Laia, G. H., Schmidta, N. W., Suna, V. Z., Rodrigueza, A. R. Tongd, R., Tangd, L., Chengd, J., Deminga, T. J., Kameia, D. T., and Wonga, G. C. L. (2011) Translocation of HIV TAT peptide and analogues induced by multiplexed membrane and cytoskeletal interactions. *Proc. Natl. Acad. Sci. USA* 108, 16883–16888.

Morris, M. C., Depollier, J., Mery. J., Heitz, F., and Divita, G. (2001) A peptide carrier for the delivery of biologically activeproteins into mammalian cells. *Nat. Biotechnol.* 19, 1173–1176.

Morris, M. C., Vidal, P., Chaloin, L., Heitz, F., and Divita, G. (1997) A new peptide vector for efficient delivery of oligonucleotides into mammalian cells, *Nucleic Acids Res.* 25, 2730–2736.

Nagle, J. F. and Tristram-Nagle, S. (2000) Structure of lipid bilayers, *Biochim. Biophys. Acta*, 1 469, 159-195.

Needham, D., and Nunn, R. S. (1990) Elastic deformation oand failure of lipid bil;ayer membranes containing cholesterol, *Biophys. J*. 58, 997-1009.

Oehlke, J., Wallukat, G., Wolf, Y., Ehrlich, A., Wiesner, B., Berger, H., and Bienert, M. (2004) Enhancement of intracellular concentration and biological activity of PNA after conjugation with a cell-penetrating synthetic model peptide, *Eur. J. Biochem.* 271, 3043–3049.

Oglęcka, K., Lundberg, P., Magzoub, M., Eriksson, L. E. G., Langel, Ü., and Gräslund, A. (2008) Relevance of the N-terminal NLS-like sequence of the prion protein for membrane perturbation effects, *Biochim. Biophys. Acta.* 1778, 206–213.

Okamura, E., Ninomiya, K., Futaki, S., Nagai, Y. Kimura, T. Wakai, C., Matubayasi, N., Sugiura, Y., and Nakahara, M. (2005) Real-time In-cell 19F NMR Study on Uptake of Fluorescent and Nonfluorescent 19F-Octaarginines into Human Jurkat Cells, *Chem. Lett.* 34, 1064-1065.

Padari, K., Säälik, P., Hansen, M., Koppel, K., Raid, R., Langel, Ü., and Pooga, M. (2005), Cell Transduction Pathways of Transportans, *Bioconjugate Chem*. 16, 1399-1410.

Park, C. B., Kim, H. S., and Kim, S. C. (1998) Mechanism of action of the antimicrobial peptide buforin II: buforin II kills microorganism by penetrating the cell membrane and inhibit the cellular functions, *Biochem. Biophys. Res. Commun.* 244, 253-257.

Pooga, M., Kut, C., Kihlmark, M., Hällbrink, M., Fernaeus, S., Raid, R., Land, T., Hallberg, E., Bartfai, T. M., and Langel, Ű. (2001) Cellular translocation of proteins by transportan. *FASEB. J*. 15, 1451-1453.

Rawictz, W., Olbrich, K. C., McIntosh, T., Needham, D., and Evans, E. (2000) Effect of chain length and unsaturation on elasticity of lipid bilayers, *Biophys. J.* 79, 328-339.

Sadler, K., Eom, K. D., Yang, J. L., Dimitrova, Y. and Tam, J. P. (2002) Translocating proline-rich peptides from the antimicrobial peptide bactenecin 7, *Biochemistry* 41, 14150-14157.

Sandre, O., Moreaux, L., and Brochard-Wyart, F., (1999) Dynamics of transient pores in stretched vesicles; *Proc. Natl. Acad. Sci. USA*, 96, 10591–10596.

Saitoh, A., Takiguchi, K., Tanaka, Y., and Hotani, H. (1998) Opening-up of liposomal membranes by talin. *Proc*. *Natl*. *Acad*. *Sci*. *USA* 95, 1026-1031.

Scheller, A., Oehlke, J., Wiesner, B., Dathe, M., Krause, E., Beyermann, M., Melzig, M., and Bienert, M. (1999) Structural requirements for cellular uptake of alpha-helical amphipathic peptides, *J. Pept. Sci.* 5, 185-194.

Simeoni, F., Morris, M. C., Heitz, F., and Divita, G. (2003) Insight into the mechanism of the peptide‐based gene delivery system MPG: implications for delivery of siRNA into mammalian cells, *Nucl. Acids Res.* 31, 2717-2724.

Song, J. Kai, M., Zhanga, W., Zhang, J., Liu, L., Zhang, B., Liu, X., and Wang, R. (2011) Cellular uptake of transportan 10 and its analogs in live cells: Selectivity and structure–activity relationship studies, *Peptides* 32, 1934–1941.

Soomets, U., Lindgren, M., Gallet, X., Pooga, M, Hällbrink, M., Elmquist, A., Balaspiri, L., Zorko, M., Pooga, M, Brasseur, R., and Langel, Ű. (2000) Deletion analogues of transportan. *Biochim. Biophys. Acta* 1467, 165-176.

Stamou, D., Duschl, C., Delamarche, E., and Vogel, H. (2003) Self-assembled microarray of attolitter molecular vesicle. *Angew. Chem.* 115, 5738-57451.

Tamba, Y., Ariyama, H., Levadny, V., and Yamazaki, M. (2010) Kinetic pathway of antimicrobial peptide magainin 2-induced pore formation in lipid membranes. *J. Phys. Chem. B.* 114, 12018-12026.

Tamba, Y., Ohba, S., Kubota, M., Yoshioka, H., Yoshioka, H., and Yamazaki, M. (2007) Single GUV method reveals interaction of Tea catechin (-)-epigallocatechin gallate with lipid membranes. *Biophys. J.* 92, 3178-3194.

Tamba, Y., Terashima, H., and Yamazaki, M. (2011) A membrane filtering method for the purification of giant unilamellar vesicles. *Chem. Phys. Lipids* 164, 351-358.

Tamba, Y., and Yamazaki, M. (2005) Single giant unilamellar vesicle method reveals effect of antimicrobial peptide, magainin-2, on membrane permeability. *Biochemistry* 44, 15823-15833.

Tamba, Y., and Yamazaki, M. (2009) Magainin 2-induce pore formation in the lipid membranes depends of its concentration in the membrane interface. *J. Phys. Chem. B* 113, 4846-4852.

Tanaka, T., Sano, R., Yamashita, Y., and Yamazaki, M. (2004) Shape changes and vesicle fission of giant unilamellar vesicles of liquid-ordered phase membrane induced by lysophosphatidylcholine. *Langmuir*, 20, 9526-9534.

Terrone, D. Sang, S. L. W., Roudaia, L., and Silvius, J. R. (2003) Penetratin and related Cell-penetrating peptide can translocate across lipid bilayers in the presence of a transbilayer potential, *Biochemistry* 42, 13787-13799.

Thorén, P. E. G., Persson, D., Karlsson, M., and Nordén, B. (2000) The Antennapedia peptide penetratin translocates across lipid bilayers-the first direct observation. *FEBS Lett.* 482, 265-268.

Tints, K., Prink, M., Neuman, T., and Palm, K. (2014) LXXLL peptide convert Transportan 10 to a potent inducer of apoptosis in breast cancer cells. *Int. J. Mol. Sci.* 15, 5680-5698.

Vivès, E., Brodin, P., and Lebleu, B. (1997) A truncates HIV-1 TAT protein basic domain rapidly translocates through the plasma membrane and accumulates in the cell nucleus, *J. Biol. Chem.* 272, 16010-16017.

Wheaten, S. A., Ablan, F. D. O., Spaller, B. L., Trieu, J. M., and Almeida, P. F. (2013) Translocation of cationic amphipathic peptides across the membranes of pure phospholipid giant vesicles. *J. Amer. Chem. Soc*. 135, 16517-16525.

Yamazaki, M. (2008) The single GUV method to reveal elementary processes of leakage of internal contents from liposomes induced by antimicrobial substances. In *Advances in Planar Lipid Bilayers and Liposomes* 7, 121-142.

Yandek, L. E., Pokerny, A., Florén, A., Knoelke, K., Langel, U., and Almeida, P. F. F. (2007) Mechanism of the Cell-penetrating peptide Transportan 10 permeation of lipid bilayers, *Biophys. J.* 92, 2434-2444.

Yandek, L. E., Pokerny, A., and Almeida, P. F. F. (2008) Small change in the primary structure of Transportan 10 alter the thermodynamics and kinetics of its interaction with phospholipid vesicles. *Biochemistry* 47, 3051-3060.

Yeagle, P. L. (1985) Cholesterol and the cell membrane, *Biochim. Biophyd. Acta* 822, 267-287.

Acknowledgment

I would like to express my deep and sincere gratitude to my supervisor, Professor Masahito Yamazaki, Department of Bioscience, Graduate School of Science and Technology, Shizuoka University, for his encouragement, supervision and useful suggestions throughout this study. He gave me the opportunity to do the PhD study in this university. His wide knowledge and his logical way of thinking have been of great value for me. His understanding, encouraging and personal guidance have provided a good basis for the present thesis. His financial support for my study is gratefully acknowledged.

My warm thanks to Hirotaka Ariyama, Md. Alam Jahangir and Taka-aki Tsuboi for his valuable suggestions and friendly help. His kind support has been of great value in this study.

During this work, I have collaborated with many colleagues for whom I have great regard, and I wish to extend my warmest thanks to all of them who have helped me with my work in the Yamazaki Lab, Department of Bioscience, Graduate School of Science and Technology, Shizuoka University, Shizuoka, Japan.

I owe my special gratitude to my father, mother, and elder brother Md. Shahidul Islam. They have lost a lot due to my research abroad. Without their encouragement and understanding it would have been impossible for me to finish this thesis. My special thanks to my wife Sabrina Sharmin and two daughters Manha Samawiyah Islam & Mahdiya Juwairiyah Islam for their loving support.

Md. Zahidul Islam

Shizuoka University, Shizuoka, Japan.

August, 2015.